

Published in Journal of Geophysical Research – Atmospheres. Copyright, 1993, American Geophysical Union. Further reproduction or electronic distribution is not permitted.

Modeling biogeochemical responses of tundra ecosystems to temporal and spatial variations in climate in the Kuparuk River Basin (Alaska)

S. Le Dizès,¹ B. L. Kwiatkowski,¹ E. B. Rastetter,¹ A. Hope,² J. E. Hobbie,¹ D. Stow,² and S. Daeschner²

Received 19 June 2001; revised 1 February 2002; accepted 5 February 2002; published 15 January 2003.

[1] We used a process-based ecosystem model (Marine Biological Laboratory General Ecosystem Model (MBL-GEM III)) to predict and analyze biogeochemical responses of Arctic tundra ecosystems to past (1921–2000) and future (2001–2100) changes in climate and atmospheric CO₂ in the Kuparuk River Basin, Alaska. We first calibrated the model by deriving a single parameter set that closely simulated the response of moist tussock tundra to decade-long experimental manipulations of nutrients, temperature, light, and atmospheric CO₂ at Toolik Lake on the North Slope of Alaska. We then applied the parameterized model to the entire Kuparuk River Basin over 180 years. The model predicted that warming and drying resulted in a short-term source of CO₂ on annual timescales but resulted in a CO₂ sink on decadal timescales. These predictions are consistent with recent measurements. A time series analysis has identified that while the immediate response to warming is to release C, the response a year later is to store C. This 1-year lag is consistent with other work that has shown a similar lag in C storage and normalized difference vegetation index (NDVI) on a global scale. Our simulation results indicated that by 2100 high CO₂ and warming will increase C sequestration, mostly as a result of (1) an increase in vegetation C:N ratio, which occurs across the Kuparuk Basin, and (2) a redistribution of N from soils (with low C:N ratios) to vegetation (with high C:N ratios), which occurs mainly in ecosystems in the basin that are initially productive, dry, and warm. These results are consistent with the observation of increased shrubiness in Alaskan tundra over the past few decades. Our application of the model has been hindered by the lack of climate data for the region, especially precipitation. A number of other general issues have been identified for making progress in modeling spatial and temporal C dynamics of Arctic tundra. **INDEX TERMS:** 1610 Global Change: Atmosphere (0315, 0325); 1615 Global Change: Biogeochemical processes (4805); 1620 Global Change: Climate dynamics (3309); 1699 Global Change: General or miscellaneous; **KEYWORDS:** global change, scaling, ecosystem model, carbon sequestration, arctic tundra, climate change

Citation: Le Dizès, S., B. L. Kwiatkowski, E. B. Rastetter, A. Hope, J. E. Hobbie, D. Stow, and S. Daeschner, Modeling biogeochemical responses of tundra ecosystems to temporal and spatial variations in climate in the Kuparuk River Basin (Alaska), *J. Geophys. Res.*, 108(D2), 8165, doi:10.1029/2001JD000960, 2003.

1. Introduction

[2] Arctic ecosystems are an important component of the global carbon (C) budget. Because of cold, wet conditions and the associated slow decomposition rates, moist tussock and wet sedge tundra soils have accumulated an estimated 29–39 kg C m⁻² [Jonasson *et al.*, 2001; Shaver and Jonasson, 2001]. Globally, Arctic ecosystems contain approximately 11% of the world's soil C [McGuire *et al.*, 1995]. Future warming and changes in precipitation could

alter soil moisture, active layer depth, decomposition rates, and permafrost distribution, and lead to oxidation of the soil C. As a result, current CO₂ fluxes to the atmosphere could increase dramatically [Mitchell *et al.*, 1990].

[3] Future changes in C storage in Arctic tundra, however, will depend not only on decomposition but also on net primary production (NPP). The same conditions that result in soil C accumulation also inhibit nitrogen (N) cycling, which in turn places a strong N limitation on the rate of NPP [Chapin and Shaver, 1985]. Future changes in C storage will depend upon how the balance between the opposing processes of C release through decomposition and C storage through NPP is affected by changes in atmospheric CO₂ and climate. For example, warmer and less waterlogged soil conditions might be expected to stimulate decomposition and release C from the large soil stocks [Oechel *et al.*, 1993]. In contrast, higher CO₂ concentrations and faster N

¹The Ecosystems Center, Marine Biological Laboratory, Woods Hole, Massachusetts, USA.

²Department of Geography, San Diego State University, San Diego, California, USA.

mineralization rates could stimulate NPP more than decomposition and thereby sequester C [McKane *et al.*, 1997b].

[4] On a global scale, fluxes of CO₂ leading to a net loss of C from tundra ecosystems could increase atmospheric CO₂ concentration and promote further greenhouse warming. In the past, tundra ecosystems on the North Slope of Alaska were net sinks of atmospheric CO₂ as evidenced by the accumulated soil organic matter. Beginning in the early 1980s, there have been several shifts in the patterns of CO₂ fluxes [Oechel *et al.*, 2000]. Now, tundra ecosystems appear to be net sinks for CO₂ in summer, but large winter releases of CO₂ result in annual net sources of CO₂ to the atmosphere. To predict what the balance will be in the future, the effects of climate variability on long-term (decadal or longer) Arctic ecosystem function need to be understood [Oechel *et al.*, 2000], especially the interactions of the C and N cycles [Billings *et al.*, 1984; Shaver *et al.*, 1992; Rastetter *et al.*, 1992; McKane *et al.*, 1997a]. Four main types of C–N interactions have an important impact on the source versus sink question [Rastetter *et al.*, 1992]; C can be stored in the ecosystem if (1) N accumulates in the ecosystem, (2) the C:N ratio of vegetation increases, (3) the C:N ratio of soil increases, or (4) there is a net movement of N from soils (with a low C:N ratio) to vegetation (with a higher C:N ratio).

[5] Terrestrial ecosystems respond to a changing climate on several timescales, as illustrated by the 9-month lag in the response of C storage to increased temperature observed by Braswell *et al.* [1997], the 10-year acclimation of tundra ecosystems to changing climate observed by Oechel *et al.* [2000], and the change in land cover and shrubbiness over several decades as observed by Sturm *et al.* [2001] and Silapaswan *et al.* [2001]. Analyses of long-term responses of terrestrial ecosystems to a changing climate and atmospheric CO₂ must include responses acting on all these timescales and be able to extrapolate them over large spatial scales. Because of the high spatial and temporal variability in environmental factors and the long time required for ecosystems to fully respond, it is impossible to determine this long-term outcome of elevated CO₂ and climate change on ecosystems by using experiments alone [Rastetter *et al.*, 1992; Rastetter, 1996; Reynolds *et al.*, 1993]. Based on knowledge acquired from short-term or fine-scale studies, process-based models are useful for predicting ecosystem response to global change on larger temporal and spatial scales [Reynolds *et al.*, 1993]. The model we have used in this paper is based on the premise that the effects of atmospheric CO₂ and climate change on the spatial and temporal patterns in ecosystem C storage are strongly constrained by C–N interactions. Our analysis aims to investigate how constraints associated with C–N interactions control variability of C storage in tussock tundra through time and space.

[6] We present a study that uses a new version of the Marine Biological Laboratory General Ecosystem Model (MBL-GEM III) to evaluate historical and projected C dynamics of the Kuparuk River Basin in Alaska to spatial and temporal variations in climate. The MBL-GEM III incorporates the aggregated canopy model (ACM) as a photosynthesis module [Williams *et al.*, 1997], simpler soil and decomposition modules, and estimates a soil moisture index from precipitation data. We have run the model for

123 10 × 10 km cells at a yearly time step, from 1920 to 2100. This fine-scale approach allowed us to further test model predictions of NPP against the normalized difference vegetation index (NDVI). This modeling exercise served two goals: it predicted and analyzed the spatial–temporal response of Arctic tundra to global change and it highlighted those areas where further research would be needed for better understanding.

2. Material and Methods

2.1. Site Description

[7] The study area consists of the 9200 km² Kuparuk River Basin located on the North Slope of Alaska. The Kuparuk Basin extends from the Brooks Range, north through the foothills and coastal wet tundra to the Arctic Ocean (Figure 1). To define the watershed boundary, we used a 1 × 1 km resolution map, which estimates the basin area at 9542 km² (D. A. Walker, personal communication, University of Alaska, Fairbanks, AK). However, because modeling was undertaken at a 10 km spatial resolution, we developed a 10 × 10 km resolution map with 123 grid cells that completely encompasses the 1 × 1 km boundary (covers an area of 12300 km²). The total area covered by moist acidic tussock, nonacidic tussock, wet sedge, and shrub tundra in each 10 × 10 km grid cell was derived using a regional vegetation map with a 50 × 50 m resolution (D. A. Walker, personal communication, 2000). The vegetation in the northern section of the basin is dominated by moist nonacidic tussock and wet sedge tundra. The southern section is dominated by moist acidic tussock and shrub tundra. Combined, these four tundra types comprise about 95% of the terrestrial landscape of the Kuparuk River Basin with moist tussock tundra being the dominant tundra type in the region [Walker *et al.*, 1994].

2.2. Model Development and Description

[8] In this paper, we have used a new version of the MBL-GEM III. A series of previous papers, Rastetter *et al.* [1997] and McKane *et al.* [1997a, 1997b] used earlier versions of the model (MBL-GEM I) to investigate past and future changes in the amount of C stored in the tundra in response to increases in atmospheric CO₂, temperature, and N deposition as well as to increases or decreases in soil moisture. These investigations dealt with the response of a single type of vegetation, tussock tundra; the model was applied to the Toolik Lake site in Alaska, where long-term field experiments on the response of tussock tundra to manipulations of CO₂, temperature, light, and soil nutrients provided data for a calibration [Oechel *et al.*, 1992; Chapin *et al.*, 1995].

[9] The next step in model development was to apply MBL-GEM I spatially [Hobbie *et al.*, 1998]. This work made use of the large environmental data set collected over the entire Kuparuk Basin (9200 km²), which includes the Toolik Lake site. The calibrated MBL-GEM I was applied over five E–W bands of the region, which differed in climate and percentage distribution of three tundra types.

[10] The new MBL-GEM III uses a gross primary production (GPP) module derived from the Soil–Plant–

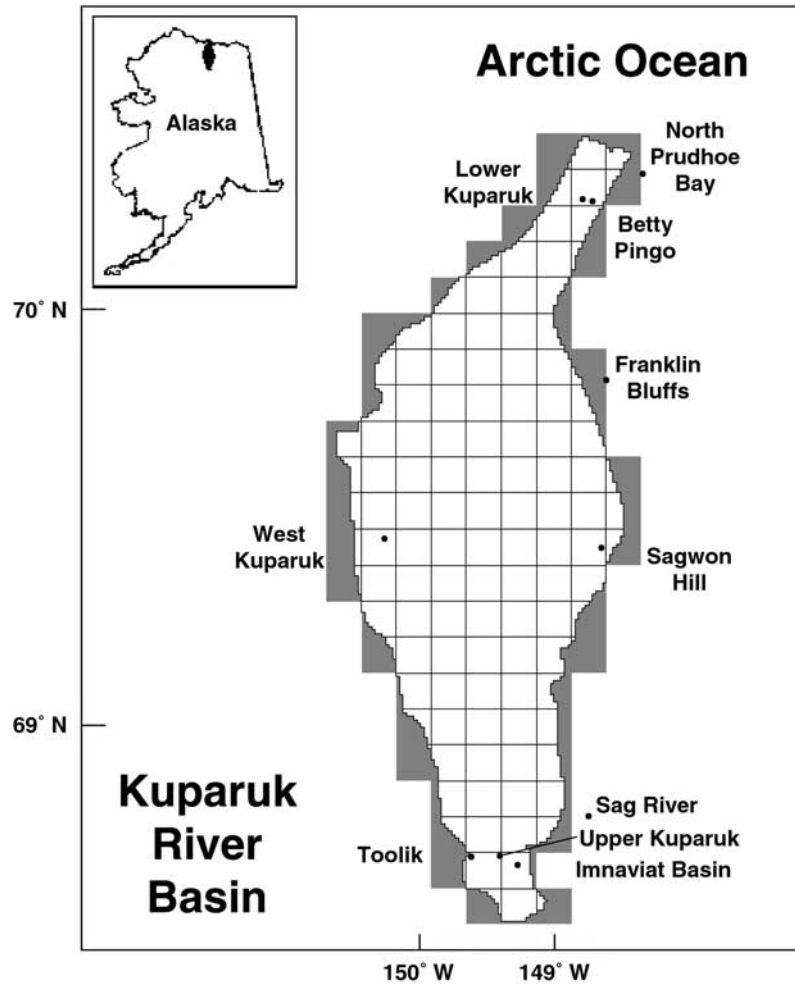


Figure 1. A map of the Kuparuk Basin, Alaska, including the watershed boundary at 1×1 km and 10×10 km resolutions and the locations of weather stations.

Atmosphere (SPA) model of *Williams et al.* [1996]. Recently, *Williams et al.* [2000] applied the SPA model to the Kuparuk Basin and tested it against ecosystem CO_2 exchange (eddy flux) data available from a N-S transect in the basin. An aggregated version of the SPA model, called ACM [*Williams et al.*, 1997] was then applied at a 1 km scale to yield the GPP for 1 year across the entire Kuparuk Basin [*Williams et al.*, 2001]. Both SPA and ACM use remote sensing information on leaf area. Because satellite data are not available for the future, these models cannot be used to predict future GPP directly. However, by using ACM as the GPP module in MBL-GEM III, this problem can be overcome.

[11] By incorporating ACM into the structure of MBL-GEM III, interactions between photosynthesis and vegetation properties (leaf area index (LAI), canopy N) are explicitly treated. On one hand, the MBL-GEM III predicts how leaf area and canopy N change in response to a changing climate; while, on the other hand, the ACM provides MBL-GEM III with an estimate of GPP consistent with eddy flux studies. This feedback between the ACM and the MBL-GEM III allows the extrapolation of photosynthesis into the future.

[12] Three other improvements have been made in the MBL-GEM III compared to the MBL-GEM I [*Rastetter et al.*, 1991]. First, the allocation scheme has been changed to shorten computation time. C and N are allocated based on the relative sink strength of the three tissues. The sink strength in each tissue decreases as labile C or N accumulates in that tissue. Second, the soil module has been simplified to treat N associated with extractives, acid soluble, and acid insoluble fractions of the soil organic matter as a single aggregated pool. The equations for decomposition processes are also somewhat simpler. Finally, the model has been modified to estimate a soil moisture index from summer precipitation rather than requiring soil moisture as an input to the model.

[13] The MBL-GEM III is a process-based, plot-scale ecosystem model of C and N interactions for the vegetation and soil components of terrestrial ecosystems (Appendix A). The model simulates stand-level photosynthesis and N uptake by plants, allocation of C and N to foliage, stems, and fine roots, respiration in these tissues, turnover of biomass through litterfall, and decomposition of litter and soil organic matter. It calculates all changes and interactions for the vegetation and soil components of terrestrial

ecosystems on an annual time step and is calibrated to run on mean growing season climate data. These data consist of mean July maximum and minimum daily air temperature, mean July daily irradiance, total growing season precipitation, mean annual CO₂ concentration, and annual N inputs in deposition. These data are organized in a Geographic Information System (GIS) to generate predictions throughout the basin. Plant season length and soil season length are treated as constant parameters in our study.

[14] The model consists of 19 simultaneous ordinary differential equations describing the temporal dynamics of 19 state variables (Appendix A). These variables represent the amounts of C and N in plant tissues (foliage, wood, roots) and in four soil organic fractions as well as the amount of soil inorganic N. Within the vegetation, both labile (readily mobilized) and structural (including enzymatic machinery and structural framework) components of foliage, stems (including sapwood), and fine roots are represented [Rastetter *et al.*, 1991]. Younger soil organic matter (including litter) is operationally partitioned into extractives (polar, i.e., extractable with hot water, and non polar, i.e., extractable with methylenechloride), acid soluble (dissolved in hot 72% H₂SO₄), and acid insoluble (the residue). Older organic matter is converted to humus with a very slow turnover rate.

[15] The model specifically includes C–N interactions. Unlike most plot-scale ecosystem models, vegetation in MBL-GEM acclimates to changes in the environment to maintain a nutritional balance between C and N [Rastetter and Shaver, 1992]. For example, changes that stimulate photosynthesis (e.g., increased CO₂ or higher irradiance) result in an increase in the relative allocation of C and N to fine roots, which in turn stimulates N uptake. Similarly, changes that stimulate N uptake (e.g., high inorganic soil N concentration) increase the relative allocation of C and N to foliage, which stimulates C uptake. Through the coupling between C and N uptake by plants, the model incorporates the biogeochemical constraints on the C budget imposed by the N cycle. A complete description of the MBL-GEM III is provided in Appendix A.

2.3. Model Calibration

[16] We calibrated the MBL-GEM III for an Arctic moist acidic tussock tundra ecosystem using the same data from long-term observations and experiments at Toolik Lake, Alaska, that were used to calibrate the MBL-GEM I [McKane *et al.*, 1997a]. The data were obtained from a 9-year study of tussock tundra responses to N and P fertilizer, 3.5°C warming using greenhouses, a combined greenhouse and fertilizer treatment, and a shade-house treatment that reduced light by 50% [Chapin *et al.*, 1995] and a 3-year experiment on net ecosystem C exchange for tussock tundra under a doubling of atmospheric CO₂ [Oechel and Riechers, 1987; Grulke *et al.*, 1990; Oechel *et al.*, 1992]. The calibration procedure we used is similar to the “top-down” approach used by McKane *et al.* [1995, 1997a], where fine-scale measurements of individual processes (e.g., tissue-level or microbial respiration) were used to estimate parameters that determine the shape of the response of a process to

changes in the environment. However, annual, plot-scale measurements (e.g., annual NPP) were used to estimate parameters that determine the rate for these processes. Because the model runs on a yearly time step and we calibrate it to multiyear dynamics of the ecosystem, the resulting parameters represent annual values, including, for example, summer plus winter respiration rates. The data and procedure that we used to calibrate the model are fully described by Chapin *et al.* [1995] and McKane *et al.* [1995, 1997a, 1997b]. After initial calibration, we optimized the parameter estimates using Monte Carlo simulations in which improved fit to all these calibration data was sought by imposing small random perturbations on the parameters. From this procedure, we derived a single parameter set for the MBL-GEM III that is simultaneously consistent with all the experimental results obtained by Chapin *et al.* [1995] (Figure 2) and with the responses to elevated CO₂ observed by Oechel *et al.* [1992] (Figure 3).

2.4. Climate Data Reconstruction

[17] We simulated C dynamics of the Kuparuk River Basin from 1921 to 2100. The climate data needed to run the model for each of the 123 grid cells representing the Kuparuk Basin were derived from data at different spatial and temporal resolutions (Table 1). Some climate data were only available through 1994 and projected forward beyond that time. We nonetheless split our analysis of past and future responses at the year 2000.

2.4.1. N Inputs and CO₂

[18] Inorganic N inputs were assumed to be 0.014 g N m⁻² yr⁻¹ for all grid cells throughout the simulations [Arctic LTER]. Atmospheric CO₂ concentration was assumed to be constant across the Kuparuk Basin, but increased from 303 mL m⁻³ in 1921 to 365 mL m⁻³ in 2000 to 730 mL m⁻³ in 2100. The pattern of increase through 1994 was based on ice core data [Enting *et al.*, 1994] and a linear doubling of atmospheric CO₂ was assumed between 1994 and 2100.

2.4.2. Air Temperature

[19] The model was calibrated to use mean daily minimum and maximum air temperatures for July. To generate these time series, we used the Hadley CM2 climate simulations as described by McGuire *et al.* [2000] for the mean July temperature of the Toolik grid cell (Figure 4). To extrapolate spatially, we used measured data to derive regressions relating the mean July temperature at 12 weather stations dispersed in the Kuparuk River Basin (Figure 1) to the Toolik mean July temperature ($r^2 = 0.31$ – 0.59). These regressions were used to extrapolate the Hadley temperatures for Toolik to the other 12 sites in the basin. Next, using the same data from Toolik and the 12 weather stations, we derived regressions relating the mean daily temperature range for July at each site to the mean July temperature at that site ($r^2 = 0.35$ – 0.56). We used these regressions and the previously constructed time series for mean July temperature to construct time series (1921–2100) of mean daily minimum and maximum temperature for July at each of the sites. Finally, we constructed a time series of mean daily minimum and maximum temperature for July for each of the 123 10 × 10 km cells in the basin by

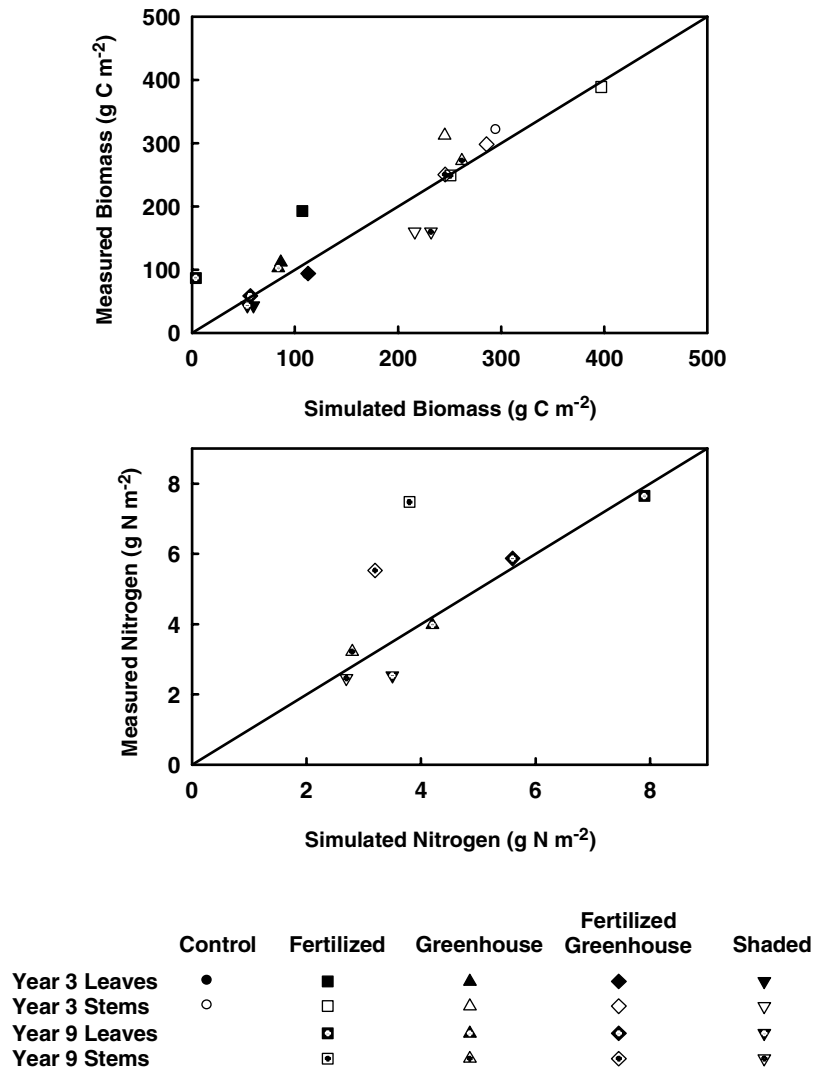


Figure 2. Measured versus simulated responses of tussock tundra vegetation at Toolik Lake to the fertilized, greenhouse, fertilized greenhouse, and shaded treatments of *Chapin et al.* [1995]. There were no measured N data for year 3. The fertilized treatments received $10 \text{ g N m}^{-2} \text{ yr}^{-1}$ as NH_4NO_3 and $5 \text{ g P m}^{-2} \text{ yr}^{-1}$ as triple superphosphate. The greenhouse treatments increased mean growing season temperature by 3.5°C . The shaded treatment decreased light by 50%.

interpolating from the time series for the 12 weather stations plus Toolik using the inverse distance-weighting interpolation routine of Arcview Spatial Analyst (Arcview GIS 3.2, ESRI, Redlands, CA, USA).

2.4.3. Irradiance

[20] The spatial–temporal coverage of radiation data in the Kuparuk Basin for the historical period was too sparse for any reliable interpolation. We instead estimated irradiance for the full simulation period (1921–2100) using a three-parameter empirical relationship derived by *Williams et al.* [2001] relating irradiance to temperature range and extraterrestrial radiation (Appendix B) [*Bristow and Campbell*, 1984].

2.4.4. Precipitation

[21] The precipitation data set used in our simulations was derived by *McGuire et al.* [2000]. These data, obtained at a $0.5^\circ \times 0.5^\circ$ (latitude \times longitude) resolution,

were converted to a $10 \times 10 \text{ km}$ resolution prior to running the model, by splitting larger grid cells as necessary. This precipitation data set indicated an increase in precipitation during the projected period. For contrast, we also simulated the effects of a future dry climate, assuming a linear decrease in precipitation of the same magnitude as the increase in wet scenario. These two scenarios enabled us to investigate the effects of two opposing climate change scenarios for the projected period: warmer and wetter (“wet scenario”) and warmer and drier (“dry scenario”).

2.5. Simulation Protocol

[22] We applied the model one grid cell at a time at the $10 \times 10 \text{ km}$ resolution (Figure 1). We assumed that there are no interactions between adjacent grid cells. Because the model equations are difficult to invert, we ran MBL-GEM

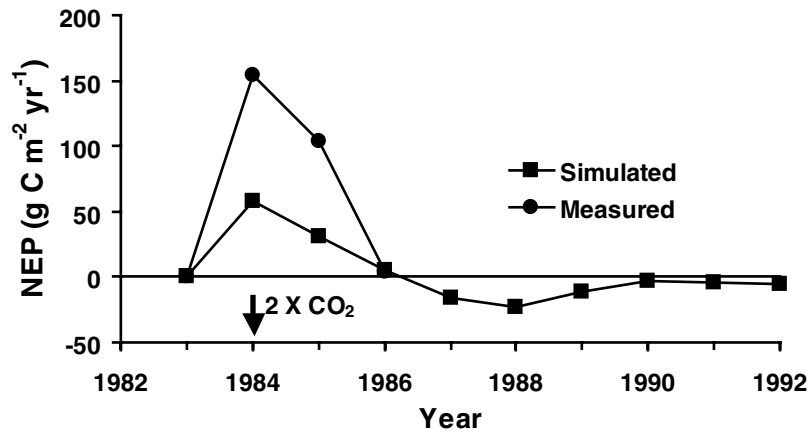


Figure 3. Measured versus simulated short-term changes in net ecosystem flux of tussock tundra at Toolik Lake in response to an instantaneous increase in atmospheric CO₂ from 344 to 680 mL m⁻³ (annual values). The CO₂ treatment was maintained for three consecutive growing seasons as described by *Oechel and Riechers* [1987], *Grulke et al.* [1990], and *Oechel et al.* [1992]. Positive fluxes indicate an increase in ecosystem C. Oechel et al. annual estimates are probably high because the magnitude of winter respiration was underestimated at the time of the experiment. The magnitude of the MBL-GEM response is based on the CO₂ response of the *Farquhar and von Caemmerer* [1982] model. The magnitude of the NEP response is probably lower in our simulations because the LAI and nitrogen content the MBL-GEM III was calibrated to were probably lower than in the plots of Oechel et al.

III to steady state for each grid cells, using the reconstructed 1921–1925 average climate. When a steady state was reached, the climate drivers varied yearly in accordance with the reconstructed climate.

2.6. Satellite Data

[23] Net primary productivity predicted by the model was compared to the NDVI. The NDVI was calculated from NOAA Advanced Very High Resolution Radiometer (AVHRR) satellite imagery as a half-monthly, maximum value composite to reduce the atmospheric effects and cloud

problems [Holben, 1986]. Maximum value compositing (MVC) is the most common form of NDVI compositing used to produce NDVI time series data sets [Eidenshink and Faundeen, 1994]. AVHRR images collected during a selected compositing period were geographically registered and the maximum observed NDVI was assigned to each pixel location for the final composite. The NDVI has been shown to be a good measure of the light capturing capacity of vegetation for photosynthesis and has been used in a variety of models to calculate ecosystem C exchange [Potter et al., 1993]. Consequently, seasonal integration of

Table 1. Climate Input Variables for MBL-GEM Simulations: Description of Spatial and Temporal Resolution, Temporal Scope, and Sources or Hypothesis Made for Each Variable

Variable	Spatial resolution	Temporal resolution	Temporal scope	Sources and hypothesis
Atmospheric CO ₂	Constant	6 months	1921–2000	Ice core measurements and atmospheric CO ₂ observations [Enting et al., 1994]
Inorganic N	Constant	Constant	2001–2100	Doubling of atmospheric CO ₂
Air temperature	10 × 10 km	July average	–	Arctic LTER online database
			1921–2100	McGuire et al. [2000] for the Toolik Lake grid cell Inverse Distance Weighting interpolation method for the whole Kuparuk
Irradiance	10 × 10 km	July average	1921–2100	Empirical relationship with temperature range [Bristow and Campbell, 1984]
Precipitation	0.5° latitude × 0.5° longitude	Growing season total	1921–2000	McGuire et al. [2000]
			2001–2100	Wet scenario: McGuire et al. [2000], Dry scenario: linear decrease of the same magnitude as wet scenario increase

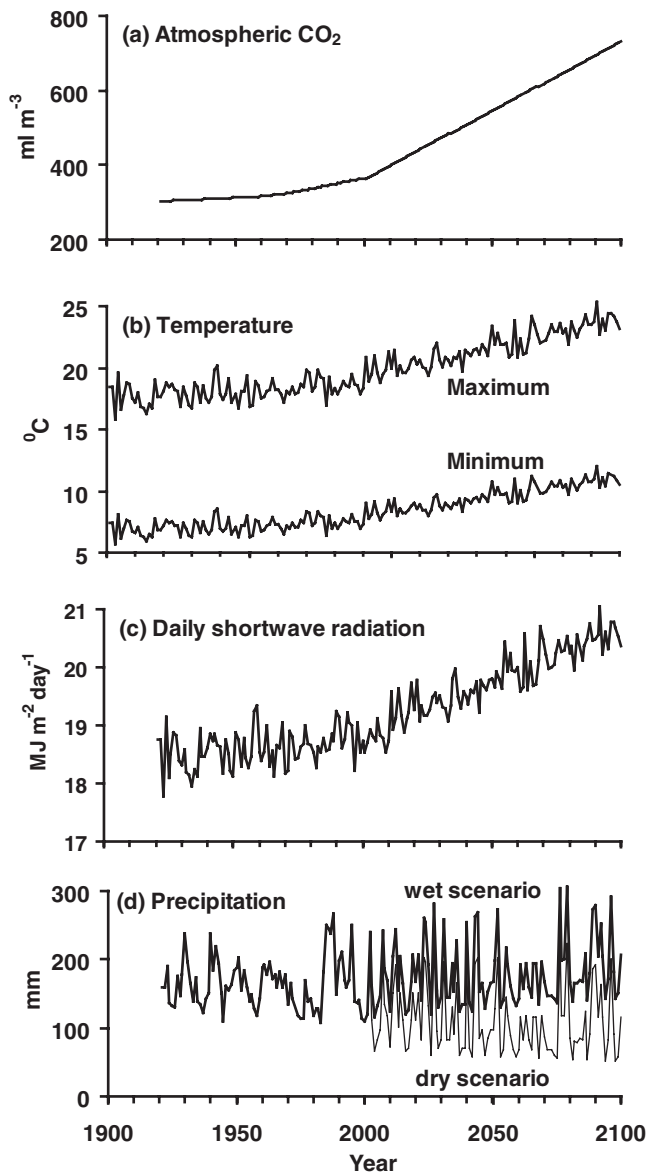


Figure 4. Historical and projected time series for (a) atmospheric CO₂ [Enting *et al.*, 1994], (b) maximum and minimum temperature, (c) daily short-wave radiation, and (d) precipitation for the Toolik Lake grid cell [McGuire *et al.*, 2000].

the NDVI (SINDVI) time series over a growing season has been correlated with ecosystem NPP [Goward and Dye, 1987]. A subset of NDVI images has been produced for the Kuparuk River Basin vegetation map for the period 1989–1996. Because precipitation has such a strong effect on our model results and the only precipitation data we have is at a 0.5° latitude × 0.5° longitude resolution, we aggregated both the SINDVI and simulated NPP to 0.5° resolution for comparison.

3. Results

[24] We first used the calibrated MBL-GEM III and the reconstructed climate data set to estimate and compare

net primary productivity against SINDVI data of Arctic tundra across the Kuparuk Basin. We then used the model to analyze temporal and spatial changes in C storage in response to historical (1921–2000) and projected changes (2001–2100) in atmospheric CO₂ and climate.

3.1. Kuparuk Basin Net Primary Productivity

[25] We used seasonally integrated NDVI (SINDVI) data for the Kuparuk Basin to corroborate model predictions of NPP for the years 1992, 1995, 1996, and 1998. Among those years, 1995 was a dry year while the other years were average. All simulations used the moist acidic tussock tundra calibration at Toolik Lake. However, there are three other major types of vegetation dispersed in the Kuparuk Basin: shrub tundra, wet sedge and moist non-acidic tussock tundra [Walker *et al.*, 1994]. To calculate the NPP for these three types of vegetation, we used the field measurements to calculate the ratio of NPP for each tundra type to the NPP of moist acidic tussock tundra. This ratio is equal to 1.20 for wet sedge tundra [Oechel and Billings, 1992], 1.49 for shrub tundra [Oechel and Billings, 1992], and 0.84 for the moist nonacidic tussock tundra (L. Gough and G. Shaver, personal communication, 2000). We then used these ratios to estimate NPP for each 10 × 10 km grid cell by multiplying the NPP for moist acidic tundra times this ratio times the fractional cover for the respective tundra type in the grid cell and summed the results.

[26] Because precipitation has such a strong effect on our simulated NPP and the precipitation data were available only at 0.5° latitude × 0.5° longitude resolution (Table 1), we aggregated both the SINDVI and NPP data to this coarser resolution (16 aggregated cells) for comparison. With this aggregation, the modeled NPP captured between 88% and 94% of the pattern in SINDVI (Table 2). A large portion of the spatial pattern in NPP predicted by the model was related to the distribution of vegetation types within the basin. If the climate is assumed uniform across the basin, so that spatial patterns in modeled NPP are due only to the distribution of vegetation, then the model captures between 80% and 83% of the variation in SINDVI (Table 2). On the other hand, if the vegetation is assumed homogeneous across the basin, so that spatial patterns in modeled NPP are due only to spatial variation

Table 2. Coefficient of Regression (r^2) Between SINDVI Data and Modeled NPP in the 16 0.5° Resolution Grid Cells of the Kuparuk Basin

Year	Regression between SINDVI and modeled NPP corrected for the spatial distribution of vegetation within the basin	Regression between SINDVI and modeled NPP corrected for the spatial distribution of vegetation, but assuming a homogeneous climate across the basin	Regression between SINDVI and modeled NPP with spatial variation in climate, but assuming a homogeneous vegetation cover throughout the basin
1992	0.94	0.83	0.87
1995	0.94	0.82	0.88
1996	0.92	0.83	0.83
1998	0.88	0.80	0.82

in climate, then the model captures between 82 and 88% of the variation in SINDVI. Clearly, both vegetation distribution and climatic variation had important effects on the spatial patterns of NPP. However, these two effects cannot be completely segregated because locations in the basin that have climates that are conducive to high productivity within a particular vegetation type are also those areas that have a high proportion of the more productive types of vegetation. Nevertheless, we took these high correlations between the SINDVI and the model to partially corroborate our predictions.

3.2. Simulated Temporal Changes of the C Budget for the Toolik Lake Grid Cell

[27] In this section we analyze past and future predictions of acidic tussock tundra NPP, soil respiration (R_H), and net ecosystem productivity ($NEP = NPP - R_H$) for the Toolik Lake grid cell alone. During the historical period (1921–2000), variations in NEP indicate that moist tussock tundra ecosystem was a net sink of CO_2 during the time period 1970–1979 and then became a net source of CO_2 (Figure 5c). This timing of the NEP response is consistent with measurements of *Oechel et al.* [2000]. Nevertheless, our model predicted only small year-to-year variations in NEP during the historical period, indicating much smaller sources and sinks in our simulations than observed by *Oechel et al.* (-28 to $+21$ $g\ C\ m^{-2}\ yr^{-1}$ in our simulations versus -450 to $+120$ $g\ C\ m^{-2}\ yr^{-1}$ in *Oechel et al.* measurements).

[28] During the projected period (2000–2100), R_H increased more in the dry scenario than in the wet scenario (Figure 5b), because the soils became less waterlogged. However, the higher soil activity also released N, which stimulated plant growth so that NPP was higher in the dry scenario (Figure 5a). Because the stimulation of NPP was greater than the increase in R_H , the rate of C sequestration (NEP) increased more in the dry scenario than in the wet scenario (Figure 5c). The cumulative effect of changes in NEP after 180 years was to increase ecosystem C stocks by 198 and 322 $g\ C\ m^{-2}$ in the wet and dry scenario, respectively (i.e., an increase of 1.8% and 3.0% above initial stocks) (Figure 6).

[29] To better understand what controls the temporal changes in ecosystem C storage, we assessed the short-term (year-to-year) effects of climate on tundra C budgets. To make this assessment, we first removed the long-term trends in the time series for precipitation, average temperature, GPP, plant respiration, NPP, R_H , and NEP by subtracting the previous year's value in each time series from the current year's value ("backward differencing," removing the trend by subtracting a high-order polynomial fit to each data series yields similar results) [*Box and Jenkins*, 1976]. We then calculated the cross correlation between each C-flux variable and each of the two climate variables (Figure 7). After removing the long-term trends, the cross correlation for the wet and dry scenarios were virtually identical (data not shown for the dry scenario); that is, long-term trends in precipitation did not affect the short-term responses of the simulated tundra C budgets.

[30] The analysis indicated that temperature had strong effects on all components of the C budget in the current and

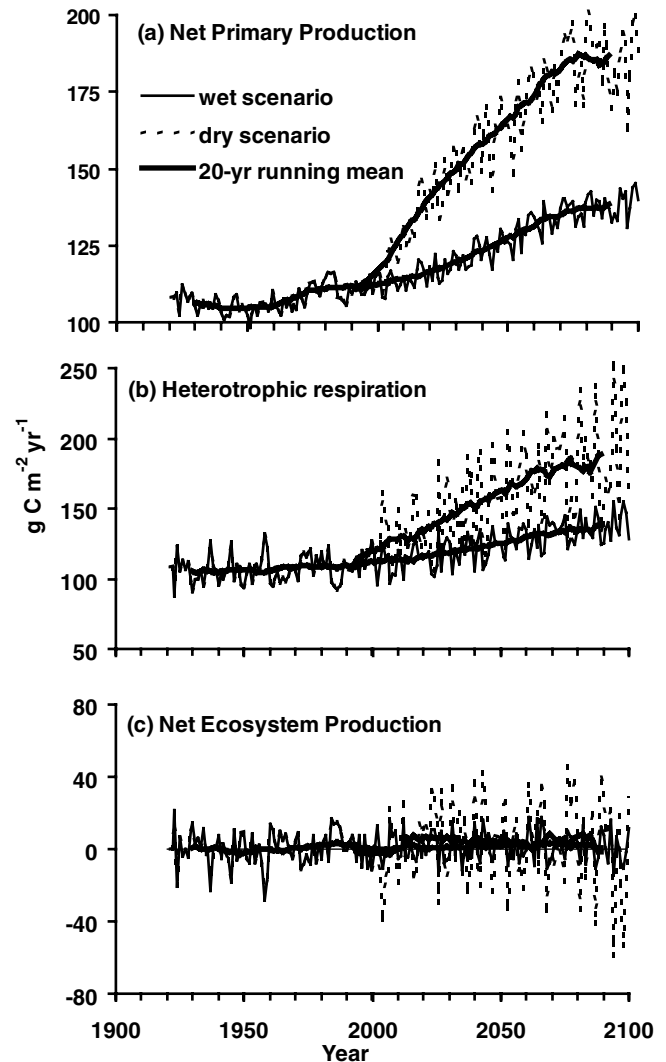


Figure 5. Simulated historical and projected changes in (a) net primary production (NPP), (b) heterotrophic respiration (R_H), and (c) net ecosystem production (NEP) in the Toolik grid cell in response to the two climate scenarios.

following years (lag = 0 and 1), but not after 2 years. Direct effect of high temperatures is to stimulate GPP and plant and soil respiration. Because respiration is more sensitive to high temperature than GPP in these cold adapted systems, the net effect of temperature on NPP and NEP is negative. The directions of these effects of temperature on the C budget reversed between the current and following year (Figure 7). This 1-year lag is consistent with the results reported by *Braswell et al.* [1997] that C storage appears to lag temperature by 9 months at the global scale. *Braswell et al.* also found a similar lag for NDVI for specific vegetation types.

[31] The major effect of high precipitation is to slow decomposition and hence R_H by further waterlogging the soil. This slowing of soil processes decreases N mineralization, which in turn slows NPP. Because R_H is slowed more than NPP, the net effect of high precipitation is to increase

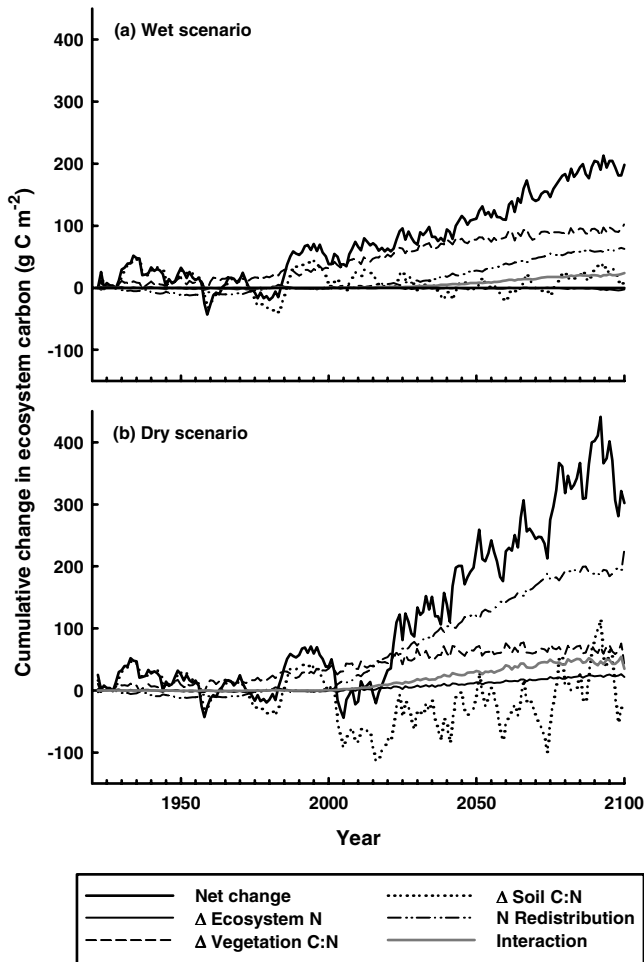


Figure 6. Simulated historical and projected changes in total ecosystem C stocks of tussock tundra (“Net change”) at Toolik Lake partitioned among three biogeochemical factors and their interaction for the (a) wet climate scenario and (b) dry climate scenario. “ Δ Ecosystem N” is the simulated change in ecosystem C associated with gains or losses of total ecosystem N, “ Δ Vegetation C:N” and “ Δ Soil C:N” are the changes associated with changes in the C:N ratio of vegetation and soil, respectively, “N redistribution” is the change associated with the redistribution of N from soil to vegetation, and “Interaction” is the change associated with the interaction of all four factors.

NEP in the current year. No lagged effect was observed in the simulations.

[32] The long-term effects of climate (over 180 years) on plant productivity and NEP were opposite to the current-year effects, especially as it relates to wetting and drying. The main drivers for the long-term pattern was the redistribution of N from soils to vegetation (see below) and the increase in woody tissues (with high C:N ratios), which both require time. Thus, there is a long lag associated with the redistribution in N and increase in woodiness. The long-term results suggested that this lagged effect eventually comes to dominate the ecosystem C budget.

[33] Additional insight into the controls of the temporal C storage in tussock tundra can be gained by analyzing changes in the C–N interactions. A key assumption of our analysis was that, for strongly N-limited ecosystems like the Alaskan tundra, changes in C storage through time interact strongly with changes in the N cycle [Shaver *et al.*, 1992; Rastetter *et al.*, 1992]. In particular, because the production and accumulation of organic matter require both C and N, ecosystems can only increase C storage by (1) accumulating new N from external sources, (2) increasing the C:N ratio of vegetation, (3) increasing the C:N ratio of soils, and (4) redistributing N from soils (with

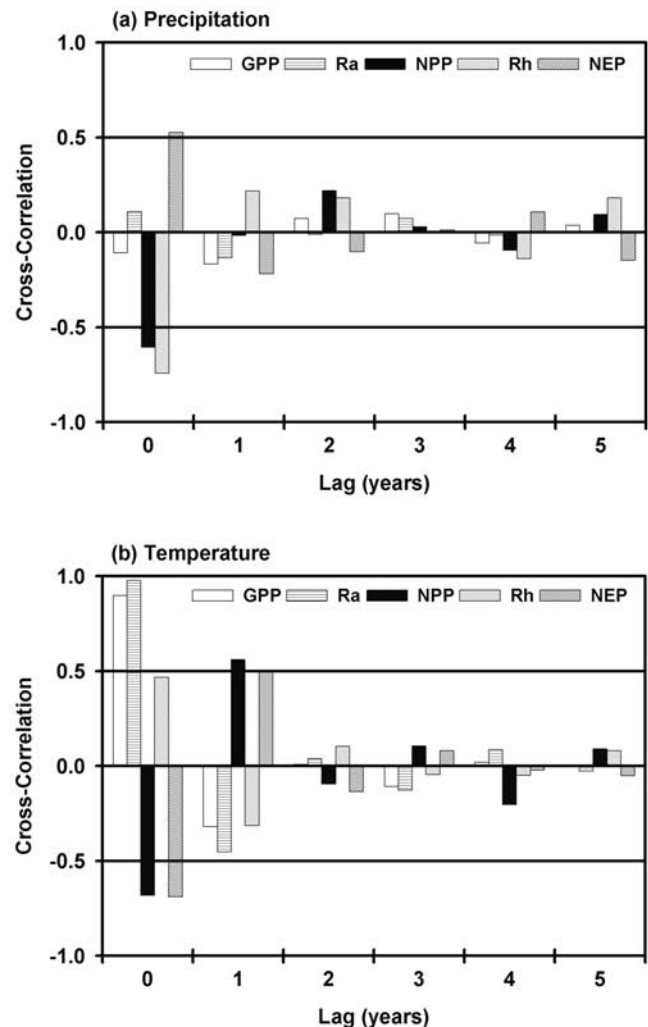


Figure 7. Cross-correlation analysis of each C flux variable against (a) precipitation and (b) temperature for the wet scenario after removing the long-term trends in the time series for each flux or climate variables. The cross correlation for the dry scenario has shown virtually identical patterns. R_a = autotrophic (plant) respiration, R_H = Heterotrophic (soil) respiration, GPP = gross primary production, NPP = net primary production ($=GPP - R_a$), and NEP = net ecosystem productivity ($NPP - R_H$).

a low C:N ratio) to vegetation (with a higher C:N ratio). Each factor (and an interactive term) was mathematically described as an independent contributor and the sum of the calculated contributions accounts for the total change in ecosystem C stocks [Rastetter *et al.*, 1992]. We used these equations to analyze how the four factors and their interaction regulated the predicted temporal changes in ecosystem C stocks. Because changes in the C–N interactions were the same for the two climate scenarios during the historical period and were relatively small compared to the projected period, we focused this analysis on the projected period.

[34] During the projected period, the two most important factors regulating long-term ecosystem C storage in response to both climate scenarios were the redistribution of N from soils to vegetation and the increase in the vegetation C:N ratio (Figure 6). Warmer temperatures stimulate the decomposition and therefore the release of both C and N from the soil. This release of N increases available N and stimulates NPP. The coupling of increased temperature with decreased soil moisture in the dry scenario amplified the increase in decomposition and the subsequent N uptake into vegetation. The vegetation C:N ratio increased in both climate scenarios as a result of an increase in woodiness under warmer and high CO₂ conditions. By 2100 in the dry scenario, the redistribution of N from soils to vegetation and the increase in the vegetation C:N ratio accounted for a net C storage in the ecosystem of 193 and 75 g C m⁻², respectively. In the wet scenario, these two factors accounted for 63 and 102 g C m⁻², respectively.

[35] The next most important factor regulating long-term C storage in response to both climate scenarios was the change in the C:N ratio of soils. The C:N ratio of organic matter generally declines as it decomposes. The C:N ratio of soils reflects a balance between this decrease in the C:N ratios of individual litter cohorts as they decompose and the input of fresh litter with a relatively high C:N ratio. Losses in C stocks associated with decreased soil C:N ratios were more important under the dry scenario than the wet scenario. In the dry scenario, the model predicted that the amount of C stored in soils per unit N declined before 2075, resulting in a negative contribution to the net change in ecosystem C stocks (Figure 6). However, after 2075, increased litter inputs by plants had again increased the soil C:N ratio, so that its contribution to net C storage was positive. A wet period beginning about in 2075 also contributed to this increase in soil C:N ratio.

[36] The least important factor controlling the long-term predicted increase in C storage was the change in the total ecosystem N. In the wet scenario, a very small amount of N was lost from the ecosystem by 2100 because of increased

leaching under the wetter conditions. In the dry scenario, ecosystem N increased through time because of lower leaching losses and because of a high N demand associated with both greater vegetation biomass and a higher immobilization potential associated with larger litter inputs to the soil.

[37] Finally, the interaction among the four factors contributed positively to the overall C budget. In both scenarios the important interaction was between the redistribution of N from soil to vegetation and the increase in the vegetation C:N ratio. As both of these factors increase through time, the interactive effect of moving soil N into a woodier vegetation was positive in both scenarios.

3.3. Simulated Spatial Changes in Ecosystem C Storage

[38] In this section, we analyze spatial differences of C storage in vegetation, soil, and the total ecosystem between 1921 and 2000 (historical period) and between 2000 and 2100 (projected period) for acidic tussock tundra across the Kuparuk Basin.

[39] It is difficult to predict future responses based on the relatively small changes in the past. The model indicates that future changes will be much larger than anything experienced in the past. The changes in C storage in vegetation, soil, and thereby the total ecosystem between 1921 and 2000 showed only a small spatial variability (Figure 8) because the changes in temperature, radiation, precipitation, and atmospheric CO₂ for this period were small (Figure 4). In the future, our model predicts that there will be large spatial differences in C storage in vegetation. However, the spatial variability in the large present-day stocks of soil C overwhelms any predicted change in the spatial pattern of these C stocks.

[40] Under both future scenarios, the simulations suggest larger increases in vegetation C, soil C, and total ecosystem C (Figure 8) in the central portion of the basin than either the northern or southern portions. This spatial pattern can be explained in part by higher temperatures in the central portion of the basin. For the dry scenario, lower precipitation values in the southern and central portion of the basin also contributed to the pattern. Relative to the wet scenario, C storage in vegetation for the dry scenario was higher across the whole Kuparuk Basin (Figure 8a).

[41] To further assess the spatial differences in C gain over the Kuparuk Basin over the 180-year simulations, we used the same partitioning that was used in our analysis of the temporal patterns of NEP (see section 3.2). For each cell, we first partitioned the net change in ecosystem C among the four factors (plus their interaction). We then correlated the net C change associated with each factor

Figure 8. (opposite) MBL-GEM predicted changes since 1921 in C stocks of (a) vegetation, (b) soil, and (c) total ecosystem for tussock tundra in response to climate change and atmospheric CO₂ across the Kuparuk basin (g C m⁻²). The bin sizes were selected to emphasize the spatial patterns and are not uniform. The apparent banding is related to the higher resolution used for the precipitation data. The following C stocks were assumed for 1921: soil C = 10723 g m⁻², plant C = 710 g m⁻², and ecosystem C = 11433 g m⁻².

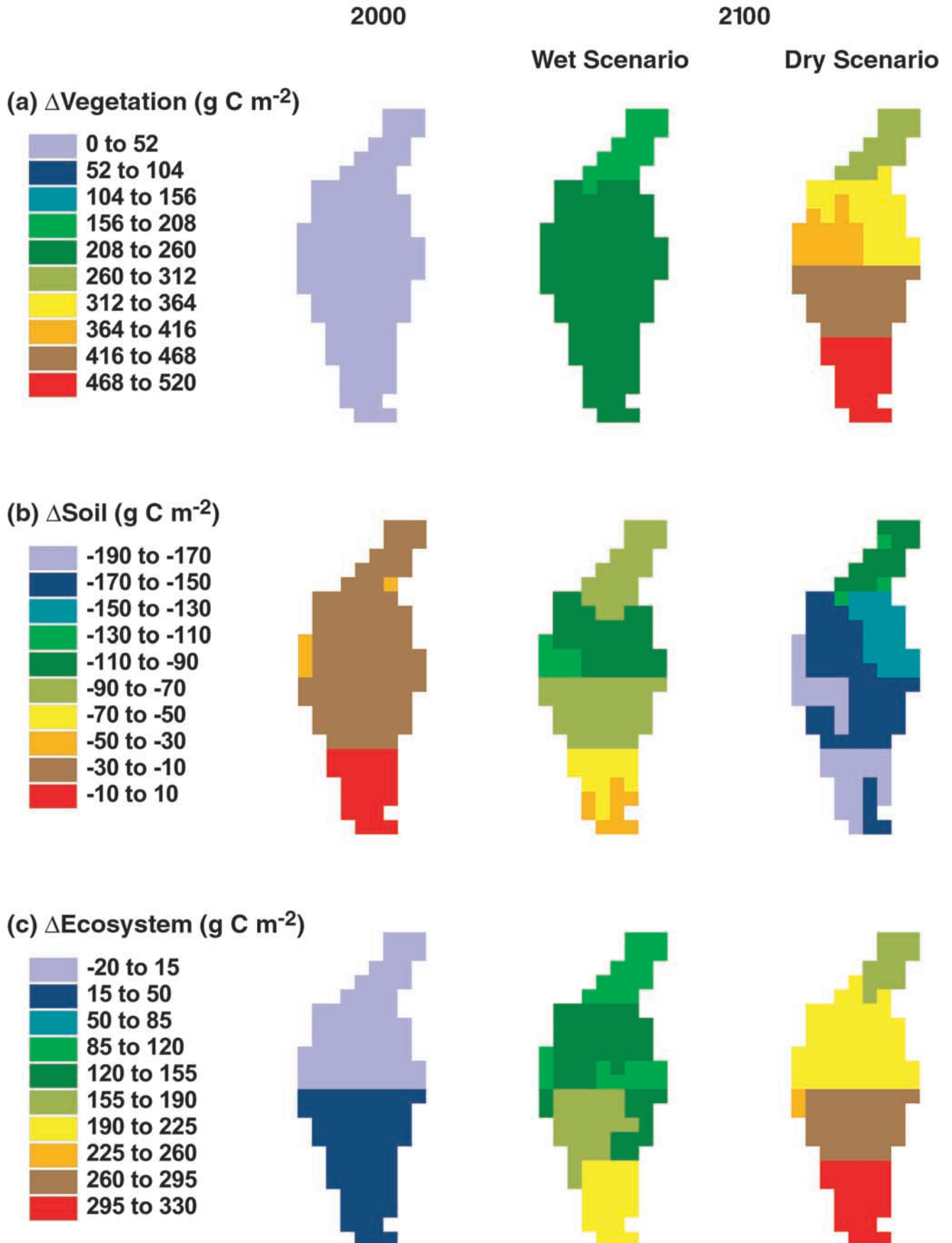


Table 3. Proportion of Variation Explained by Correlation of the Four Factors (and Their Interactive Term) of C–N Interactions With the Spatial Patterns of Initial Ecosystem Properties and Climate

	C storage (g C m ⁻²)		Initial ecosystem properties						Initial climate drivers	
	Min.	Max.	LAI	GPP	NPP	NMIN	Veg C/Soil C	Veg N/Soil N	P _{PT}	T _{air}
Wet scenario										
ΔEcosystem N	-64.28	1.27	0.57	0.43	0.58	0.60	0.33	0.39	-0.85	-0.21
ΔVegetation C:N	80.05	107.18	0.96	0.89	0.95	0.96	0.83	0.87	0.55	-0.88
ΔSoil C:N	5.013	20.88	0.37	0.21	0.32	0.39	0.11	0.20	-0.79	0.79
N redistribution	45.21	64.90	0.79	0.86	0.83	0.79	0.90	0.86	-0.93	0.55
Interaction	18.73	24.51	0.94	0.93	0.96	0.95	0.92	0.92	0.53	-0.89
Dry scenario										
ΔEcosystem N	-26.37	28.15	0.69	0.56	0.69	0.72	0.47	0.52	-0.93	-0.03
ΔVegetation C:N	74.69	84.48	-0.11	-0.02	-0.16	-0.14	0.01	0.01	-0.85	-0.15
ΔSoil C:N	-28.8	-4.17	-0.87	-0.89	-0.90	-0.87	-0.88	-0.87	-0.86	0.69
N redistribution	89.76	195.07	0.91	0.85	0.93	0.93	0.80	0.83	-0.97	0.43
Interaction	38.14	55.46	0.90	0.81	0.89	0.91	0.74	0.79	-0.86	-0.11

Note: Results are correlations of each C–N interaction factor with (1) initial ecosystem properties including leaf area index (LAI), Gross Primary Production (GPP), Net Primary Production (NPP), net N mineralization (NMIN), and ratio of vegetation to soil C and N, and (2) initial climate drivers including precipitation (P_{PT}) and average air temperature (T_{air}). Initial ecosystem properties and climate drivers were defined for the year 1921 for each grid cells. The four C–N interaction factors explaining the simulated changes in ecosystem C are defined in the text. Min. and Max. are the minimum and maximum net amount of C stored associated with each factor.

with the initial properties of the ecosystems in each cell and to the initial climate in those cells (Table 3).

[42] Across the basin, all four factors contributed significantly to the overall change in C storage in each cell (see the first two columns in Table 3). This result is in contrast to the temporal patterns at the Toolik Lake cell where N redistribution and increase in vegetation C:N ratio dominated the change in the C budget. This difference suggests that different factors control the net change in C accumulation across the basin. Some of these controls are related to the initial properties of the ecosystem, and to the initial climatic conditions.

[43] The regions of high productivity (central basin) are the regions likely to accumulate more C in the future. In both scenarios, all the initial ecosystem properties had a similar correlation to the amount of C stored associated with each of the four C–N interaction factors (Table 3). This pattern indicates that the important ecosystem property in assessing C storage was the initial productivity. All six of the ecosystem properties we examined could be related to this initial productivity. That is, high LAI, GPP, NPP, net N mineralization, and ratio of vegetation to soil C and N were all associated with highly productive tundra ecosystems.

3.3.1. Wet Scenario

[44] Under the wet scenario, some cells lost as much as 65 g C m⁻² associated with the loss of ecosystem N. This result is in contrast to the Toolik Lake cell, which lost only 3 g C m⁻² associated with this factor. The cells that lost the most C associated with N loss were the initially less productive and high-precipitation ecosystems (positive correlation with productivity and negative correlation with initial precipitation) (Table 3). High precipitation resulted in a high water flux through the soils and therefore a high potential for N loss through leaching. In addition, the low N demand of initially less productive ecosystems means they were less able to sequester N in

biomass than initially highly productive ecosystems and more N was able to leach out of the system.

[45] Regions dominated by woody vegetation have a high potential to store C in the wet scenario. For example, the cells that gained the most C associated with the increase in vegetation C:N ratio were the initially highly productive, high precipitation and cool systems (positive correlations with both productivity and initial precipitation; negative correlation with temperature) (Table 3). The reason for the increase in vegetation C:N ratio in initially productive ecosystems was a change in allocation patterns to favor wood relative to active tissues (leaves and roots), under warming and high atmospheric CO₂. Because N release from soils was lower under wetter conditions, initially high precipitation systems were not able to move as much N from the soil to the vegetation and thereby promoting higher vegetation C:N ratios.

[46] Under the wet scenario, regions of high productivity also store more C per unit N in soils because the high litter flux results in a high soil C:N ratio. Indeed, across the basin, the cells that gained the most C associated with the increase in soil C:N ratio in the wet scenario were the initially highly productive, low precipitation, and warm ecosystems (Table 3).

[47] The grid cells with the highest redistribution of N from soil to vegetation in the wet scenario were the initially productive, low precipitation, and warm systems (positive correlation with productivity and temperature; negative correlation with initial precipitation). The high N demand of vegetation in these ecosystems means plants were able to scavenge and sequester N from the soil. The potential for redistributing N from soil to vegetation was also accelerated under drier initial conditions because of the increase in N release from soils.

[48] Finally, under the wet scenario, the cells that gained the most C because of the interaction of all factors were the initially productive, high precipitation and cool systems.

The important interaction was amplified by the large N redistribution from soil to vegetation in initially productive systems. This effect was partly counteracted by a loss of N in initially high precipitation systems.

3.3.2. Dry Scenario

[49] Under the dry scenario, the cells that gained the most C associated with the sequestration of N from outside the ecosystem were the initially productive and low-precipitation ecosystems. For initially productive systems, higher N demand by soil and vegetation associated with increased NPP and litter input to the soil resulted in less N being leached out of the ecosystem. In addition, the N sequestration increased because of less leaching of N associated with lower water throughput in initially low precipitation systems.

[50] The spatial pattern of tundra responses to climate will differ if the future climate is dry versus wet. Indeed, in the dry scenario, in contrast to the wet scenario, the gain in C associated with the increase in vegetation C:N ratio was independent of initial productivity and decreased with initial precipitation rates.

[51] The cells that lost the most C associated with the decrease in the soil C:N ratio in the dry scenario were the initially productive ecosystems. These high productive ecosystems have large inputs of high C:N ratio litter to the soil. Upon drying, this C:N ratio narrows, resulting in a net loss of C per unit soil N. Wet, cool locations also tended to lose C associated with a narrowing of soil C:N ratio. Again, these systems tend to have initially high soil C:N ratios because of lower decomposition rates and these C:N ratios decline upon drying.

[52] For the same reasons as in the wet scenario, the cells that redistributed the most N from soil to vegetation were the initially productive, cool, and low precipitation systems.

[53] Finally, all cells gained between 38 and 55 g C m⁻² because of the interaction among the four factors. The effect of increased C:N ratio of vegetation was amplified by the high redistribution of N from soil to vegetation in initially productive and low precipitation systems.

4. Discussion

[54] We have used the process-based MBL-GEM III to analyze changes in C storage of Arctic tundra in the Kuparuk River Basin in response to past and future changes in atmospheric CO₂ and climate. We first calibrated the model by deriving a single parameter set that closely simulated the response of moist tussock tundra to decade-long experimental manipulations of nutrients, temperature, light and atmospheric CO₂ at Toolik Lake on the North Slope of Alaska [Chapin *et al.*, 1995; Oechel *et al.*, 1992]. The range in these variables among treatments is about as large as their anticipated changes in the Arctic in response to changes in atmospheric CO₂ and climate. We then applied the calibrated model to make 180-year projections, assuming that the relatively short-term experimental data were sufficient to constrain the parameters controlling longer-term mechanisms represented in the model. The key steps for implementing such a model are the temporal scaling from year to decadal and longer periods and the spatial scaling from plot to region.

[55] Our application of MBL-GEM III to the entire Kuparuk River Basin over 180 years has been hindered by the availability of climate data needed to drive the model at these regional and long temporal scales. In sparsely inhabited high-latitude regions such as the Kuparuk River Basin, climate records are only available at limited locations and seldom extend back more than a few decades. These locations may also provide a poor representation of regional climate patterns because they lie on the coast and at low elevations along rivers and valleys. Mountains and other inaccessible areas are not represented. Given the paucity and biased nature of climate data across the Kuparuk Basin, it is difficult to estimate reliably the temporal and regional patterns of climate.

[56] The model results were most sensitive to changes in patterns of precipitation. This sensitivity of our model to precipitation is similar to that found by Clein *et al.* [2000] and McGuire *et al.* [2000], particularly in relation to the sensitivity of soil metabolism to changes in moisture. The regional patterns of precipitation we used were derived from data at a broader scale (i.e., 0.5° latitude × 0.5° longitude resolution) than the 10 × 10 km resolution scale used in our simulations. Data at a finer scale are needed for future modeling at higher resolution.

[57] Clearly, on very long timescales (e.g., 1000 years or more), the cold, wet conditions in tundra have resulted in a large C accumulation. Our simulations indicate, however, that on decadal timescales, warming and especially drying could also result in C accumulation associated with the net movement of N released from decomposing soil organic matter (with a low C:N ratio) into vegetation (especially woody vegetation, with a high C:N ratio). Indeed, across the Kuparuk Basin, the model predicted a higher 200-year C sequestration for systems subjected to the drier climate scenario. In contrast, on very short timescales (e.g., annual), our simulations indicate that drying led to net C losses because of the direct stimulation of decomposition in these waterlogged soils. This pattern of C loss is associated with drying on annual timescales, but net storage on decadal timescales is consistent with measurements by Oechel *et al.* [1993, 2000].

[58] Because Arctic tussock tundra ecosystems are strongly N limited, we have hypothesized that four key aspects of C and N interactions constrain the spatial and temporal variability of ecosystem C storage in response to changes in atmospheric CO₂ and climate: (1) changes in the amount of N in the ecosystem, (2) changes in the C:N ratios of vegetation, (3) changes in the C:N ratios of soil, and (4) redistribution of N between soil (with a low C:N ratio) and vegetation (with a high C:N ratio). Our analysis indicated that the redistribution of N from soils to vegetation and the increase in vegetation C:N ratio were the most important factors controlling the temporal patterns of C storage for ecosystems near Toolik Lake, in both scenarios. These results are particularly important in that they are consistent with emerging information that tundra in Alaska is becoming more shrubby [Sturm *et al.*, 2001; Silapaswan *et al.*, 2001; Myneni *et al.*, 1997; Zhou *et al.*, 2001]. The soil C:N ratio also explained a part of the long-term predicted increase in C storage in the dry scenario. The other factors only played a minor role in the temporal patterns of C storage near Toolik Lake.

[59] In contrast to the temporal patterns of C storage at Toolik Lake, all four factors (and their interaction) contributed significantly to the spatial patterns of C storage across the Kuparuk Basin in both scenarios. The only exception was the increase in vegetation C:N ratio, which occurred in all cells, whatever their initial properties and climate drivers. Relative to initially less productive ecosystems, the initially productive ecosystems in the wet scenario (1) lost less C associated with losses of N from the ecosystem, (2) gained more C associated with increased C:N ratios in vegetation, (3) gained more C associated with increased C:N ratio of soils, and (4) gained more C associated with the redistribution of N from soils to vegetation. These spatial patterns of tundra responses to climate will differ if the future climate is dry versus wet. Relative to initially less productive ecosystems, the initially productive ecosystems in the dry scenario (1) gained more C associated with gains of N by the ecosystem, (2) gained about the same amount of C associated with increased C:N ratio of vegetation, (3) lost more C associated with decreased C:N ratio of soils, and (4) gained more C associated with the redistribution of N from soils to vegetation. In both scenarios, regions of high productivity and dominated by woody vegetation have a high potential to store C. However, high water flux can result in N losses that will limit C sequestration. Ecosystems in regions that are highly productive (central basin) can limit N losses and a positive feedback ensues between production and N retention.

[60] Because our model uses the same photosynthesis model as *Williams et al.* [2001], it is not surprising that our estimate of the spatial pattern of present-day production is consistent with theirs. However, because the Williams et al. model relies on NDVI or vegetation maps to estimate LAI and derive an estimate of foliar N, they were not able to project their findings into the future. The MBL-GEM III provides dynamic estimates of both LAI and foliar N and we were therefore able to project production estimates into the future.

[61] *McGuire et al.* [2000] cautioned against extrapolating climate responses from the Kuparuk River Basin directly to the whole Arctic because the combinations of the components of climate change differ regionally. Our finding that different factors associated with C–N interactions control changes in ecosystem C at different locations in the basin is consistent with the McGuire et al. finding, but at a finer spatial scale.

[62] Our spatial modeling of the Kuparuk Basin allowed us to test the predictions of NPP against the remotely sensed SINDVI. Although there is still some debate and uncertainty as to exactly what the SINDVI represents (NPP? GPP?), we assumed it was the best surrogate of plant productivity to compare with the model results. The several-year comparison between modeled NPP and SINDVI indicated that both vegetation distribution and climatic variations within the Kuparuk Basin explained a large portion of the spatial patterns of NPP predicted by the model. This comparison provided a valuable, independent check on the spatial distribution of productivity across the basin. In this respect, our study

has broken new ground in using remote sensing information to verify model dynamics in the context of retrospective analyses to gain confidence in the use of the model for making temporal as well as spatial predictions.

[63] To extrapolate our simulations of moist acidic tussock tundra across the basin, we assumed a ratio between the NPP of this tundra type and each of three other tundra types. This ratio was different for each of the three tundra types; once set, it was held constant across the entire basin. This spatial constancy could not be tested against field data. It would be worthwhile to calibrate the model to the other vegetation types and run them independently. In particular, in P-limited ecosystems such as wet sedge tundra [*Shaver et al.*, 1998], P may be more important than N in restricting changes in C storage [*Rastetter et al.*, 1992]. To analyze how these ecosystems respond to global change, it will be important in the future to better understand the P cycling and how C–P interactions might constrain the predicted increases in C storage.

[64] The vegetation distribution used in our simulations is not dynamic. However, our simulation results indicated that without the effect of climate there was a high correlation between SINDVI and the spatial distribution of vegetation. Therefore, it will be important to incorporate changes in the distribution of vegetation through time in the model for any future assessments of spatial and temporal changes in ecosystem C storage.

[65] Furthermore, our modeling approach does not consider changes in the length of the growing season or changes in winter decomposition. Substantial research is being focused on these issues, and a number of empirical studies are beginning to substantiate that the annual C balance of forests depends substantially on the timing of the spring thaw and that warmer winters may lead to higher decomposition releases [e.g., *Frolking et al.*, 1996; *Myneni et al.*, 1997; *Goulden et al.*, 1998; *Randerson et al.*, 1999; *Oechel et al.*, 1997, 2000; *Zhou et al.*, 2001]. Nevertheless, these issues represent major challenges for models to consider and additional information and understanding are needed in tundra ecosystems to address them with models.

[66] All models making long-term (e.g., 20–200 years) and broad-scale projections face a common problem: validation data are difficult or impossible to obtain at these scales [*Rastetter*, 1996]. Moreover, data derived from short-term (i.e., less than 10 years) experiments cannot be used to corroborate long-term projections as it may take many years for all feedback mechanisms to come into play [*Oechel and Strain*, 1985; *Rastetter*, 1996; *Oechel et al.*, 2000]. This situation, however, should not be an obstacle to modeling. Our model synthesizes empirical knowledge of the interactions among environmental factors and C–N interactions controlling C storage. Through this synthesis, it provides a process-based interpretation of biogeochemical responses of tussock tundra that is consistent with available information. Thus, the model has a major role in evaluating tundra ecosystem behavior in response to changes in climate and atmospheric CO₂.

Appendix A: The General Ecosystem Model

Table A1. Initial State Variables, Specified Initial Fluxes, and Parameters Used in MBL-GEM III for Tussock Tundra at Toolik Lake

Symbol	Definition	Value	Units	Reference
State variables				
C_F	Foliage structural carbon	76.5	g C m^{-2}	<i>Shaver and Chapin</i> [1991], <i>Chapin et al.</i> [1995]
C_{SW}	Sapwood structural carbon	273	g C m^{-2}	<i>Shaver and Chapin</i> [1991]
C_W	Wood structural carbon	273	g C m^{-2}	<i>Shaver and Chapin</i> [1991]
C_R	Root structural carbon	150	g C m^{-2}	Nadelhoffer, personal communication, 2000
C_{LF}	Foliage labile carbon	1.67	g C m^{-2}	calibrated
C_{LW}	Wood labile carbon	3.11	g C m^{-2}	calibrated
C_{LR}	Root labile carbon	1.96	g C m^{-2}	calibrated
C_S	Soluble soil carbon	644	g C m^{-2}	backcalculated
C_E	Extractive soil carbon	556	g C m^{-2}	backcalculated
C_I	Insoluble soil carbon	324	g C m^{-2}	backcalculated
C_H	Humus soil carbon	8980	g C m^{-2}	backcalculated
C_{ST}	Total organic soil carbon	11267	g C m^{-2}	<i>Giblin et al.</i> [1991], <i>Arctic LTER</i>
N_F	Foliage structural nitrogen	3.06	g N m^{-2}	<i>Shaver and Chapin</i> [1991], <i>Chapin et al.</i> [1995]
N_{SW}	Sapwood structural nitrogen	2.48	g N m^{-2}	<i>Shaver and Chapin</i> [1991]
N_W	Wood structural nitrogen	2.48	g N m^{-2}	<i>Shaver and Chapin</i> [1991]
N_R	Root structural nitrogen	3.36	g N m^{-2}	<i>Nadelhoffer et al.</i> [2002], Nadelhoffer, personal communication, 2000
N_{LF}	Foliage labile nitrogen	0.027	g N m^{-2}	calibrated
N_{LW}	Wood labile nitrogen	0.14	g N m^{-2}	calibrated
N_{LR}	Root labile nitrogen	0.049	g N m^{-2}	calibrated
N_A	Active soil nitrogen	2	g N m^{-2}	backcalculated
N_H	Humus soil nitrogen	398	g N m^{-2}	backcalculated
N_{ST}	Total organic soil nitrogen	400	g N m^{-2}	<i>Giblin et al.</i> [1991], <i>Arctic LTER</i>
N_{NH4}	Soil inorganic nitrogen	0.3	g N m^{-2}	<i>Giblin et al.</i> [1991], <i>Arctic LTER</i>
Initial driver variables				
C_a	Carbon dioxide	355	ppm	G. Kling, personal communication, 2000
D_{NH4}	Inorganic N inputs	0.0141	$\text{g N m}^{-2} \text{ yr}^{-1}$	<i>Arctic LTER</i>
I	Daily incident short-wave radiation	15.6	$\text{MJ m}^{-2} \text{ d}^{-1}$	<i>Arctic LTER</i>
P_{PT}	Summer precipitation	0.162	m yr^{-1}	<i>Arctic LTER</i>
S_p	Plant season length	100	days	<i>Arctic LTER</i>
S_s	Soil season length	100	days	Assumed equal to S_p
T_{amax}	Maximum daily temperature	16.9	$^{\circ}\text{C}$	<i>Arctic LTER</i>
T_{amin}	Minimum daily temperature	6.8	$^{\circ}\text{C}$	<i>Arctic LTER</i>
Initial fluxes				
NPP_F	Foliage NPP	50.4	$\text{g C m}^{-2} \text{ yr}^{-1}$	<i>Shaver and Chapin</i> [1991]
NPP_W	Wood NPP	26	$\text{g C m}^{-2} \text{ yr}^{-1}$	<i>Shaver and Chapin</i> [1991]
NPP_R	Root NPP	25	$\text{g C m}^{-2} \text{ yr}^{-1}$	<i>Nadelhoffer et al.</i> [2002]
P_s	Photosynthesis	260	$\text{g C m}^{-2} \text{ yr}^{-1}$	1995 estimate using the ACM [<i>Williams et al.</i> , 1997]
U_{NH4}	Plant N Uptake	1.503	$\text{g N m}^{-2} \text{ yr}^{-1}$	<i>Shaver and Chapin</i> [1991]
T_N	N translocation	1.293	$\text{g N m}^{-2} \text{ yr}^{-1}$	<i>Shaver and Chapin</i> [1991]
Plant processes				
a_{GCF}	C_F growth C coefficient	0.192	g N m^{-2}	calibrated
a_{GCW}	C_W growth C coefficient	0.009	g N m^{-2}	calibrated
a_{GCR}	C_R growth C coefficient	0.011	g N m^{-2}	calibrated
a_{GNF}	N_F growth C coefficient	0.260	g N m^{-2}	calibrated
a_{GNW}	N_W growth C coefficient	0.248	g N m^{-2}	calibrated
a_{GNR}	N_R growth C coefficient	0.015	g N m^{-2}	calibrated
a_{NF}	Leaf N photosynthesis conversion factor	0.54	unitless	<i>Shaver and Chapin</i> [1991], <i>Williams and Rastetter</i> [1999]
a_{SE}	Soluble to extractives C rate constant	0.0009	d^{-1}	calibrated
a_{EI}	Extractives to insoluble C rate constant	0.004	d^{-1}	calibrated
a_{IE}	Insoluble to extractives C rate constant	0.007	d^{-1}	calibrated
a_{IH}	Insoluble to humus rate C constant	0.001	d^{-1}	calibrated
a_H	Humus decay constant	3.63×10^{-5}	d^{-1}	backcalculated
a_{TCF}	Foliage C voltage coefficient	11.6	yr^{-1}	backcalculated
a_{TCW}	Wood C voltage coefficient	6.85	yr^{-1}	calibrated
a_{TCR}	Root C voltage coefficient	3.83	yr^{-1}	backcalculated
a_{TNF}	Foliage N voltage coefficient	39.7	yr^{-1}	backcalculated
a_{TNW}	Wood N voltage coefficient	22.0	yr^{-1}	calibrated
a_{TNR}	Root N voltage coefficient	52.7	yr^{-1}	backcalculated
a_{τ}	Translocation fraction	0.65	unitless	<i>Shaver and Chapin</i> [1991]
a_{WR}	Wood respiration correction factor	0.5	unitless	Ryan, personal communication, 1998
b_{GCF}	C_F growth N coefficient	0.075	g C m^{-2}	calibrated
b_{GCW}	C_W growth N coefficient	0.274	g C m^{-2}	calibrated
b_{GCR}	C_R growth N coefficient	0.096	g C m^{-2}	calibrated
b_{GNF}	N_F growth N coefficient	0.069	g C m^{-2}	calibrated
b_{GNW}	N_W growth N coefficient	0.126	g C m^{-2}	calibrated

Table A1. (continued)

Symbol	Definition	Value	Units	Reference
b_{GNR}	N_R growth N coefficient	0.052	$g\ C\ m^{-2}$	calibrated
E_p	Potential evaporation	0.73	$m\ H_2O\ yr^{-1}$	calibrated
g_{CFm}	C allocation maximum for leaf growth	7.330	yr^{-1}	backcalculated
g_{CWm}	C allocation maximum for wood growth	0.225	yr^{-1}	backcalculated
g_{CRM}	C allocation maximum for root growth	0.752	yr^{-1}	backcalculated
g_{NFm}	N allocation maximum for leaf growth	0.281	yr^{-1}	backcalculated
g_{NWM}	N allocation maximum for wood growth	0.003	yr^{-1}	backcalculated
g_{NRM}	N allocation maximum for root growth	0.009	yr^{-1}	backcalculated
h_1	sapwood parameter	5	$m^2\ grd\ m^{-2}\ leaf$	calibrated
h_2	sapwood parameter	0.99	–	calibrated
K_{Ca}	Foliage–stem C conductance	5.07	unitless	calibrated
K_{Cb}	Stem–root C conductance	5.94	unitless	calibrated
K_{CF}	Foliage C conductance	1	unitless	calibrated
K_{CW}	Wood C conductance	1	unitless	calibrated
K_{CR}	Root C conductance	1	unitless	calibrated
k_{CO2}	Photosynthesis half saturation constant	500.3	ppm	Williams, personal communication, 2001
k_{GCF}	C_F growth half saturation constant	0.043	$g\ C\ g\ N\ m^{-4}$	calibrated
k_{GCW}	C_W growth half saturation constant	0.320	$g\ C\ g\ N\ m^{-4}$	calibrated
k_{GCR}	C_R growth half saturation constant	0.231	$g\ C\ g\ N\ m^{-4}$	calibrated
k_{GNF}	N_F growth half saturation constant	0.010	$g\ C\ g\ N\ m^{-4}$	calibrated
k_{GNW}	N_W growth half saturation constant	0.017	$g\ C\ g\ N\ m^{-4}$	calibrated
k_{GNR}	N_R growth half saturation constant	0.114	$g\ C\ g\ N\ m^{-4}$	calibrated
K_{Na}	Foliage–stem N conductance	20.0	unitless	calibrated
K_{Nb}	Stem–root N conductance	68.6	unitless	calibrated
K_{NF}	Foliage N conductance	1	unitless	calibrated
K_{NW}	Wood N conductance	1.29	unitless	calibrated
K_{NR}	Root N conductance	1	unitless	calibrated
m_F	Foliage carbon density	79	$g\ C\ m^{-2}\ leaf$	Shaver and Chapin [1991]
p	Evapotranspiration parameter	0.00136	$mm^{-1}\ H_2O$	calibrated
q_I	Target C:N for ins–act N	22.6	$g\ C\ g^{-1}\ N$	backcalculated
r_g	Growth respiration coefficient	0.25	unitless	calibrated
r_m	Metabolic respiration constant	60.00	$g\ C\ g\ N^{-1}\ yr^{-1}$	backcalculated
S_c	GPP scaling parameter	0.71	unitless	backcalculated
T_{Rmax}	Maximum temperature for respiration	50	$^{\circ}C$	calibrated
T_{Ropt}	Optimum temperature for respiration	35	$^{\circ}C$	calibrated
x_1	Calibrated parameter for ACM	0.192		Williams, personal communication, 2001
x_2	Calibrated parameter for ACM	0.125		Williams, personal communication, 2001
x_5	Calibrated parameter for ACM	2.196		Williams, personal communication, 2001
x_6	Calibrated parameter for ACM	50.41		Williams, personal communication, 2001
x_7	Calibrated parameter for ACM	0.161		Williams, personal communication, 2001
x_8	Calibrated parameter for ACM	14.78		Williams, personal communication, 2001
x_9	Calibrated parameter for ACM	1.146		Williams, personal communication, 2001
γ_R	Respiration temperature response curvature	0.135	$(^{\circ}C)^{-1}$	calibrated
κ_L	Plant hydraulic resistance	1	$mmol\ m^{-2}\ s^{-1}\ MPa^{-1}$	Williams et al. [2001]
Ψ_f	Field potential	0.1	MPa	Dunne and Leopold [1978, p.174]
Ψ_w	Wilting potential	2.5	MPa	Dunne and Leopold [1978, p.174]
Γ^*	CO_2 compensation point	0.468		Williams, personal communication, 2001
Litterfall				
$a_{\lambda F}$	Foliage litterfall rate	0.644	yr^{-1}	backcalculated
$a_{\lambda W}$	Wood litterfall rate	0.0941	yr^{-1}	backcalculated
$a_{\lambda R}$	Root litterfall rate	0.164	yr^{-1}	backcalculated
Soil processes				
J_{dmax}	Decomposition fraction at maximum H_2O	0.15	unitless	calibrated
k_{Im}	N Immobilization half saturation constant	11.3	$\mu mol\ N\ L^{-1}$	calibrated
k_{NH4}	NH_4 uptake half saturation constant	12.8	$\mu mol\ N\ L^{-1}$	calibrated
N_{NH4mx}	Maximum NH_4 sorbed to soil	5.59×10^{-5}	$g\ N\ g^{-1}\ dry\ soil$	backcalculated
N_{NH4s}	NH_4 sorbed to soil particles	212.00	$g\ N\ m^{-2}$	calibrated
q_{uo}	Minimum allowable root C/N	10.5	$g\ C\ g^{-1}\ N$	calibrated
Q_{10D}	Soil respiration Q_{10}	2	unitless	calibrated
U_{NH4max}	Maximum plant uptake rate of NH_4	7.59×10^{-3}	d^{-1}	backcalculated
V_{Imax}	N immobilization maximum	1.14×10^{-4}	$g\ N\ m^{-2}\ d^{-1}$	backcalculated
W_{dmin}	Decomposition minimum soil H_2O	31.71	mm H_2O	calibrated
W_{dopt}	Decomposition optimum soil H_2O	71.4	mm H_2O	calibrated
W_f	Soil water at field capacity	2.3	$g\ H_2O\ g^{-1}\ dry\ soil$	Arctic LTER
W_w	Soil water at wilting point	1.16	$g\ H_2O\ g^{-1}\ dry\ soil$	Arctic LTER
z	Soil depth	0.37	m	Arctic LTER
β	Soil respiration efficiency	0.2	unitless	calibrated
Δ	Site latitude	68.5	degrees	Arctic LTER
φ_d	Decomposition moisture skewness	0.1	unitless	calibrated
ρ	Soil density	150.000	$g\ m^{-3}$	Arctic LTER

Notes: Variables and parameters for which references are provided were constrained by experimental data. “Backcalculated” variables and parameters were calculated to be consistent with the assumption of year-to-year equilibrium in C and N stocks. “Calibrated” parameters were adjusted to provide a best fit to the experimental data of Chapin et al. [1995] (fertilized, greenhouse, fertilized greenhouse, and shade treatments) and Oechel et al. [1992] (CO_2 treatment).

Table A2. Variables Used in MBL-GEM III

Symbol	Definition	Units
Plant processes		
C_m	Mesophyll CO_2 concentration	ppm
D_L	Number of hours of daylight	hours
E_T	Evapotranspiration	$m\ H_2O\ yr^{-1}$
g_c	Stomatal conductance to CO_2	$g\ C\ m^{-2}\ ppm^{-1}\ d^{-1}$
G_{CX}	C allocation to growth of tissue X	$g\ C\ m^{-2}\ yr^{-1}$
G_{CLX}	C allocation to labile tissue X	$g\ C\ m^{-2}\ yr^{-1}$
G_{NX}	N allocation to growth of tissue X	$g\ N\ m^{-2}\ yr^{-1}$
G_{NLX}	N allocation to labile tissue X	$g\ N\ m^{-2}\ yr^{-1}$
H_R	Respiration temperature response function	unitless
L_{AI}	LAI of the canopy	$m^2\ leaf\ m^{-2}\ gnd$
P_D	Conductance-corrected photosynthesis	$g\ C\ m^{-2}\ d^{-1}$
P_N	Photosynthetic potential	$g\ C\ m^{-2}\ d^{-1}$
P_{II}	Light-corrected photosynthesis	$g\ C\ m^{-2}\ d^{-1}$
q_{Xmin}	Minimum C:N ratio of tissue X	$g\ C\ g^{-1}\ N$
R_{Xmet}	Metabolic respiration of tissue X	$g\ C\ m^{-2}\ yr^{-1}$
R_{Xgr}	Growth respiration of tissue X	$g\ C\ m^{-2}\ yr^{-1}$
V_{CX}, V_{NX}	Potential at the circuit node opposite tissue X	$g\ C\ m^{-2}\ yr^{-1}$ or $g\ N\ m^{-2}\ yr^{-1}$
Litterfall and translocation		
λ_{CLX}	Litterfall C from labile pool of tissue X	$g\ C\ m^{-2}\ yr^{-1}$
λ_{CX}	Litterfall C from structural pool of tissue X	$g\ C\ m^{-2}\ yr^{-1}$
λ_{CXT}	Total litterfall C of tissue X	$g\ C\ m^{-2}\ yr^{-1}$
λ_{NLX}	Litterfall N from labile pool of tissue X	$g\ N\ m^{-2}\ yr^{-1}$
λ_{NX}	Litterfall N from structural pool of tissue X	$g\ N\ m^{-2}\ yr^{-1}$
λ_{NXT}	Total litterfall N of tissue X	$g\ N\ m^{-2}\ yr^{-1}$
τ_N	Translocation of total N from foliage	$g\ N\ m^{-2}\ yr^{-1}$
τ_{NS}	Translocation of structural N from foliage	$g\ N\ m^{-2}\ yr^{-1}$
τ_{NL}	Translocation of labile N from foliage	$g\ N\ m^{-2}\ yr^{-1}$
Litterfall fractionations		
F_{CAE}	input of C into soil extractive pool	$g\ C\ m^{-2}\ yr^{-1}$
F_{CAI}	input of C into soil acid-insoluble pool	$g\ C\ m^{-2}\ yr^{-1}$
F_{CAS}	input of C into soil acid-soluble pool	$g\ C\ m^{-2}\ yr^{-1}$
Soil processes		
A_w	Available water fraction	unitless
F_{CEI}	Flux of C from extractive to insoluble soil pool	$g\ C\ m^{-2}\ yr^{-1}$
F_{CIE}	Flux of C from insoluble to extractive soil pool	$g\ C\ m^{-2}\ yr^{-1}$
F_{CIH}	Flux of C from insoluble to humus soil pool	$g\ C\ m^{-2}\ yr^{-1}$
F_{CSE}	Flux of C from soluble to extractive soil pool	$g\ C\ m^{-2}\ yr^{-1}$
F_{NAH}	Flux of N from active soil to humus soil pool	$g\ N\ m^{-2}\ yr^{-1}$
F_{NAI}	Gross N mineralization from active soil	$g\ N\ m^{-2}\ yr^{-1}$
F_{NHI}	Gross N mineralization from humus	$g\ N\ m^{-2}\ yr^{-1}$
F_{NIA}	N immobilization into active soil	$g\ N\ m^{-2}\ yr^{-1}$
J_d	Decomposition soil moisture response function	unitless
N_{NH4aq}	NH_4 concentration in soil water	$\mu mol\ N\ L^{-1}$
Q_W	Soil water discharge	$m\ yr^{-1}$
Q_{NH4}	NH_4 loss by leaching	$g\ N\ m^{-2}\ yr^{-1}$
q_u	minimum root C:N ratio active in N uptake	$g\ C\ g^{-1}\ N$
r_s	Soil respiration temperature factor	days yr^{-1}
R_E	respiration from active soil	$g\ C\ m^{-2}\ yr^{-1}$
R_H	respiration from humus	$g\ C\ m^{-2}\ yr^{-1}$
W	Soil water	$mm\ H_2O$
ϵ	Tension slope	unitless
Ψ_d	Water potential difference between soil and leaf	MPa

Tissue X refers to foliage (F), wood (W), or root (R).

Table A3. Differential Equations Used in GEM to Simulate Changes in C and N Stocks

Changes in Carbon stocks ($g\ C\ m^{-2}\ yr^{-1}$)	Changes in Nitrogen stocks ($g\ N\ m^{-2}\ yr^{-1}$)
$\frac{dC_F}{dt} = G_{CF} - \lambda_{CF} - R_{Fgr}$	$\frac{dN_F}{dt} = G_{NF} - \lambda_{NF} - \tau_{NS}$
$\frac{dC_W}{dt} = G_{CW} - \lambda_{CW} - R_{Wgr}$	$\frac{dN_W}{dt} = G_{NW} - \lambda_{NW}$
$\frac{dC_R}{dt} = G_{CR} - \lambda_{CR} - R_{Rgr}$	$\frac{dN_R}{dt} = G_{NR} - \lambda_{NR}$
$\frac{dC_{LF}}{dt} = G_{CLF} - G_{CF} - \lambda_{CLF}$	$\frac{dN_{LF}}{dt} = G_{NLF} - G_{NF} - \lambda_{NLF} - \tau_{NL}$
$\frac{dC_{LW}}{dt} = G_{CLW} - G_{CW} - \lambda_{CLW}$	$\frac{dN_{LW}}{dt} = G_{NLW} - G_{NW} - \lambda_{NLW}$
$\frac{dC_{LR}}{dt} = G_{CLR} - G_{CR} - \lambda_{CLR}$	$\frac{dN_{LR}}{dt} = G_{NLR} - G_{NR} - \lambda_{NLR}$
$\frac{dC_S}{dt} = F_{CAS} - F_{CSE}$	$\frac{dN_A}{dt} = \lambda_{NL} + \lambda_{NW} + \lambda_{NR} + F_{NIA} - F_{NAH} - F_{NAI}$
$\frac{dC_E}{dt} = F_{CAE} + F_{CSE} + F_{CIE} - F_{CEI} - R_E$	$\frac{dN_H}{dt} = F_{NAH} - F_{NHI}$
$\frac{dC_I}{dt} = F_{CAI} + F_{CEI} - F_{CIE} - F_{CIH}$	$\frac{dN_{NH4}}{dt} = F_{NAI} + F_{NHI} + D_{NH4} - U_{NH4} - Q_{NH4} - F_{NIA}$
$\frac{dC_H}{dt} = F_{CIH} - R_H$	

t refers to the time step of the calculation, i.e., 1 year. Variables are listed in Table A2 and process equations are given in Tables A4–A10.

Table A4. ACM Equations, Variables, and Parameters Incorporated in the Structure of MBL-GEM III as a Photosynthesis Module

$$P_N = \frac{x_1 a_{NF} N_F}{g_c} \frac{x_8 T_{\max}}{x_8 + T_{\max}} \quad g_c = \frac{|\Psi_d|}{r_L + 0.5(T_{\max} - T_{\min})} \quad \frac{P_N(C_m - \Gamma^*)}{k_{CO_2} + (C_m - \Gamma^*)} = g_c(C_a - C_m)$$

$$P_D = g_c(C_a - C_m) \quad P_{II} = \frac{x_7 P_D L_{AI}^2 I}{P_D L_{AI}^9 + E_0 L_{AI}^2 I} \quad P_s = S_c S_P (x_2 D_L + x_5) P_{II}$$

The ACM is fully described in *Williams et. al* [1997]. All parameters and variables are defined in Tables A1 and A2.

Table A5. Equations, Variables, and Parameters Used to Simulate Metabolic and Growth Respiration Components in the Different Tissues

$$H_R = e^{\gamma_R (T_a - T_{Ropt})} \left(\frac{T_{Rmax} - T_a}{T_{Rmax} - T_{Ropt}} \right)^{\gamma_R} (T_{Rmax} - T_{Ropt}) \quad q_{Xmin} = \frac{g_{Cxm} b_{GNX}}{g_{NXm} b_{GCX}}$$

$$R_{Xmet} = r_m H_R \min \left(N_X, \frac{C_X}{q_{Xmin}} \right), X = F \text{ or } R \quad R_{Xgr} = \frac{r_g G_{CX}}{1 + r_g}$$

$$R_{Wmet} = r_m a_{WR} H_R \min \left(N_{sw}, \frac{C_{sw}}{q_{Wmin}} \right) \quad C_{SW} = \min(C_W, h_1 L_{AI} C_W^{h_2}) \quad N_{SW} = C_{SW} \frac{N_W}{C_W}$$

X refers to foliage (F), wood (W), or root (R) unless noted differently.

Table A6. Equations Used to Simulate C and N Allocation to the Labile and Structural Pools of the Three Tissues

$$G_{CLX} = K_{CX}(V_{CX} - a_{TCX} C_{LX}) \quad G_{NLX} = K_{NX}(V_{NX} - a_{TNX} N_{LX})$$

$$P_s = G_{CLR} + R_{Fmet} + K_{Ca}(V_{CF} - V_{CW}) \quad U_{NH4} = G_{NLR} + K_{Nb}(V_{NR} - V_{NW})$$

$$K_{Ca}(V_{CF} - V_{CW}) = G_{CLW} + R_{Wmet} + K_{Cb}(V_{CW} - V_{CR}) \quad K_{Nb}(V_{NR} - V_{NW}) + \tau_N = G_{NLW} + K_{Na}(V_{NW} - V_{NF})$$

$$K_{Cb}(V_{CW} - V_{CR}) = G_{CLR} + R_{met} \quad K_{Na}(V_{NW} - V_{NF}) = G_{NLF}$$

$$G_{CX} = \frac{g_{Cxm} C_X C_{LX} N_{LX}}{k_{GCX} + a_{GCX} C_{LX} + b_{GCX} N_{LX} + C_{LX} N_{LX}} \quad G_{NX} = \frac{g_{NXm} C_X C_{LX} N_{LX}}{k_{GNX} + a_{GNX} C_{LX} + b_{GNX} N_{LX} + C_{LX} N_{LX}}$$

X refers to foliage (F), wood (W), or root (R). All parameters and variables are defined in Tables A1 and A2.

Table A7. Equations Describing Litter Production, Translocation, and N Uptake

$$\lambda_{CLX} = a_{NX} C_{LX} \quad \lambda_{NLF} = \lambda_{CLF} (1 - a_\tau) \frac{N_{LE}}{C_{LF}} \quad \lambda_{NSF} = \lambda_{CF} (1 - a_\tau) \frac{N_F}{C_F}$$

$$\lambda_{CSX} = a_{NX} C_X \quad \lambda_{NLX} = \lambda_{CLX} \frac{N_{LX}}{C_{LX}}; \mathbf{X} = \mathbf{W} \text{ or } \mathbf{R} \text{ only} \quad \lambda_{NSX} = \lambda_{CX} \frac{N_X}{C_X}; \mathbf{X} = \mathbf{W} \text{ or } \mathbf{R} \text{ only}$$

$$\tau_{NS} = a_\tau a_{XF} N_F \quad \tau_{NL} = a_\tau a_{XF} N_{LF} \quad \tau_N = \tau_{NS} + \tau_{NL}$$

$$q_u = \min \left(q_{u0}, \frac{C_u}{N_r} \right) \quad U_{NH4} = \frac{S_p U_{NH4max} C_R N_{NH4aq}}{q_u (k_{NH4} + N_{NH4aq})}$$

X refers to foliage (F), wood (W), or root (R). All parameters and variables are defined in Tables A1 and A2. Dissolved NH₄ (N_{NH4aq}) is described in Table A10.

Table A8. Equations Describing the Extractives, Acid Soluble, and Acid Insoluble Fractions of Incoming Litter

$$F_{CNE} = \sum_x 0.36 (1 - e^{-120/q_{\lambda x}}) \lambda_{CXT} \quad q_{\lambda x} = \frac{\lambda_{CXT}}{\lambda_{NXT}}$$

$$F_{CNS} = \left(\sum_x \lambda_{CXT} \right) - F_{CNE} - F_{CNI} \quad F_{CNI} = \sum (0.35 - 0.15 e^{-50/q_{\lambda x}}) \lambda_{CXT}$$

Table A9. Equations Describing Organic Matter and Soil N Transformations

$$r_s = S_S J_d Q_{10D}^{T_s/10} \quad J_d = J_{dmax} \left[\frac{w^{q_d} - w^{q_{dopt}}}{w^{q_{dopt}} - w^{q_{dmin}}} \right]^2$$

$$F_{CSE} = r_s a_{SE} C_S \quad F_{NAI} = r_s a_{IE} N_A$$

$$F_{CEI} = r_s a_{EI} C_E \quad F_{NIA} = \frac{r_s V_{imax} N_{NH4aq}}{k_{im} + N_{NH4aq}} \left(\frac{C_I}{N_A} - q_I \right); \text{if } \frac{C_I}{N_A} > q_I$$

$$F_{CIE} = r_s a_{IE} C_I \quad = 0; \text{otherwise}$$

$$F_{CIH} = r_s a_{IH} C_I \quad F_{NAH} = r_s a_{IH} \frac{C_I}{q_I}$$

$$R_E = r_s \beta (a_{SE} C_S + a_{IE} C_I + a_{EI} C_E) \quad F_{NHI} = r_s a_{HI} N_H$$

$$R_H = r_s a_{HI} C_H$$

Table A10. Equations Used to Simulate Soil Water and NH₄ Leaching

$W = 70 + (126 - 70)(1 - e^{-14P_{PT}})$	$\overline{P_{PT}} = \frac{1000P_{PT}}{S_p}$	$Q_W = P_{PT}^{-Er}$
$\varepsilon = \ln\left(\frac{\psi_w}{\psi_f}\right)$	$A_w = \frac{10^3 W - W_w}{W_w - W_w}$	$\Psi_d = \psi_w(1 - e^{-\varepsilon A_w})$
$N_{NH4aq} = 0.5 \left\{ \frac{N_{NH4} - \rho z N_{NH4ms}}{1.4 \times 10^{-5} W} - \eta_{NH4} + \sqrt{\left(\frac{N_{NH4} - \rho z N_{NH4ms}}{1.4 \times 10^{-5} W} - \eta_{NH4} \right)^2 + \frac{4\eta_{NH4} N_{NH4}}{1.4 \times 10^{-5} W}} \right\}$		
$N_{NH4s} = N_{NH4} - 1.4 \times 10^{-5} W N_{NH4aq}$		$Q_{NH4} = 1.4 \times 10^{-2} Q_W N_{NH4aq}$

Appendix B: Solar Radiation Interception

[67] The spatial–temporal coverage of radiation data in the Kuparuk basin for the historical 1921–2000 period was too sparse for any reliable interpolation. We instead used an empirical relationship between daily incident radiation and daily temperature range using a modified version by *Bristow and Campbell* [1984]:

$$I = k_0 j_1 (1 - (\exp - j_2 (T_{amax} - T_{amin})^{j_3}))$$

where k_0 is the extraterrestrial radiation and (j_1 , j_2 , j_3) are parameters derived for July 1995 from the Toolik data set by *Williams et al.* [2001].

[68] The extraterrestrial radiation (k_0) is defined as followed:

$$k_0 = 0.0864 S_0 \left(\frac{s}{24} \sin(\delta) \sin(\Delta) + \frac{1}{\pi} \cos(\Delta) \cos(\delta) \sin\left(\frac{s\pi}{24}\right) \right)$$

where S_0 is a solar constant (1360 W m^{-2}), Δ is the latitude, s is the daylength (hours), and δ is the solar declination:

$$s = 24 \cos^{-1}(-\tan(\Delta) \tan(\delta)) / \pi \quad \text{if } \tan(\Delta) \tan(\delta) \geq 1 \text{ then } s = 24$$

$$\delta = -23.4 \cos\left(\frac{360(D + 10)}{365} - \frac{\pi}{180}\right) \quad \text{where } D = \text{Julian Day}$$

[69] In our analysis, k_0 was calculated using the midbasin latitude (i.e., $\Delta = 69.5^\circ \text{N}$) and averaged over July 1995 (i.e., D between 182 and 212). We assumed that the parameter set (j_1 , j_2 , j_3 , k_0) was constant across the basin and over the duration of the simulation (Table B1).

Table B1. Values of the Constant Parameter Set (j_1 , j_2 , j_3 , k_0) Derived for July 1995 From the Toolik Data Set by *Williams and Rastetter* [1999]

Parameter	Value
k_0	39.67
j_1	1.52
j_2	0.06
j_3	0.76

[70] **Acknowledgments.** We thank D. Walker (University of Alaska Fairbanks) for the vegetation type cover map and L. Hinzman for the temperature data. Funding was provided by grants from the National Science Foundation (NSF-LTER 0221000 and NSF-OPP 9732281).

References

Arctic LTER, Arctic LTER online database at <http://ecosystems.mbl.edu/ARC/2000>.

- Box, G. E. P., and G. M. Jenkins, *Time Series Analysis, Forecasting and Control (Revised Edition)*, Holden-Day, Boca Raton, Fla., 1976.
- Billings, W. D., K. M. Peterson, O. J. Luken, and D. A. Mortensen, Interaction of increasing atmospheric carbon dioxide and soil nitrogen on the carbon balance of tundra microcosms, *Oecologia*, 65, 26–29, 1984.
- Braswell, B. H., D. S. Schimel, E. Linder, and P. B. Moore, The response of global terrestrial ecosystems to interannual temperature variability, *Science*, 278, 870–872, 1997.
- Bristow, K. L., and G. S. Campbell, On the relationship between incoming solar radiation and daily maximum and minimum temperature, *Agric. For. Meteorol.*, 31, 159–166, 1984.
- Chapin, F. S., III, and G. R. Shaver, Individualistic growth response of tundra plant species to environmental manipulations in the field, *Ecology*, 66, 564–576, 1985.
- Chapin, F. S., III, G. R. Shaver, A. E. Giblin, K. J. Nadelhoffer, and J. A. Laundre, Responses of arctic tundra to experimental and observed changes to climate, *Ecology*, 76, 694–711, 1995.
- Clein, J. S., B. L. Kwiatkowski, A. D. McGuire, J. E. Hobbie, E. B. Rastetter, J. M. Melillo, and D. W. Kicklighter, Modeling carbon responses of tundra ecosystems to historical and projected climate: A comparison of a plot- and a global-scale ecosystem model to identify process-based uncertainties, *Global Change Biol.*, 6, S127–S140, 2000.
- Dunne, T., and L. B. Leopold, *Water in Environmental Planning*, 818 pp., W. H. Freeman, New York, 1978.
- Eidenshink, J. C., and J. L. Faundeen, The 1 km AVHRR global land data set—first stages in implementation, *Int. J. Remote Sens.*, 15, 443–462, 1994.
- Enting, I., T. Wigley, and M. Heimann, Future emissions and concentrations of carbon dioxide: Key ocean/atmosphere/land analyses, *CSIRO Div. of Atmos. Res. Tech. Pap.* 31, 120 pp., 1994.
- Farquhar, G. D., and S. von Caemmerer, Modeling photosynthetic response to the environment, in *Physiological Plant Ecology II, Encycl. of Plant Physiol., New Ser.*, vol. 12B, edited by O. L. Lange et al., pp. 459–587, Springer-Verlag, New York, 1982.
- Frolking, S., et al., Modeling temporal variability in the carbon balance of a spruce/moss boreal forest, *Global Change Biol.*, 2, 343–366, 1996.
- Giblin, A. E., K. J. Nadelhoffer, G. R. Shaver, J. A. Laundre, and A. J. McKerrow, Biogeochemical diversity along a riverside topequence in Arctic Alaska, *Ecol. Monogr.*, 61, 415–435, 1991.
- Goulden, M. L., J. W. Munger, S.-M. Fan, B. C. Daube, and S. C. Wofsy, Exchange of carbon dioxide by a deciduous forest: Response to inter-annual climate variability, *Science*, 279, 210–217, 1998.
- Goward, S. N., and D. G. Dye, Evaluating North America net primary productivity with satellite observations, *Adv. Space Res.*, 7, 165–174, 1987.
- Grulke, N. E., G. H. Riechers, W. C. Oechel, U. Hjelm, and C. Jaeger, Carbon balance in tussock tundra under ambient and elevated atmospheric CO₂, *Oecologia*, 83, 485–494, 1990.
- Hobbie, J. E., B. L. Kwiatkowski, E. B. Rastetter, D. A. Walker, and R. B. McKane, Carbon cycling in the Kuparuk River Basin: Plant production, carbon storage, and sensitivity to future changes, *J. Geophys. Res.*, 103, 29,065–29,073, 1998.
- Holben, B. N., Characteristics of maximum-value composite images from temporal AVHRR data, *Int. J. Remote Sens.*, 7, 1417–1434, 1986.
- Jonasson, S., F. S. Chapin III, and G. R. Shaver, Biogeochemistry in the Arctic: Patterns, Processes, and Controls, in *Global Biogeochemical Cycles in the Climate System*, edited by E. D. Schulze, S. P. Harrison, M. Heimann, E. A. Holland, J. J. Lloyd, I. C. Prentice, and D. Schimel, pp. 139–150, Academic Press, San Diego, Calif., 2001.
- McGuire, A. D., J. M. Melillo, D. W. Kicklighter, and L. A. Joyce, Equilibrium responses in soil carbon to climate change: Empirical and process-based estimates, *J. Biogeogr.*, 22, 785–796, 1995.
- McGuire, A. D., J. S. Clein, J. M. Melillo, D. W. Kicklighter, R. A. Meier, C. J. Vorosmarty, and M. C. Serreze, Modeling carbon responses of tundra ecosystems to historical and projected climate: Sensitivity of Pan-Arctic carbon storage to temporal and spatial variation in climate, *Global Change Biol.*, 6, 141–159, 2000.

- McKane, R. B., E. B. Rastetter, J. M. Melillo, G. R. Shaver, C. S. Hopkinson, and D. N. Fernandes, Effects of global change on carbon storage in tropical forests of South America, *Glob. Biogeochem. Cycles*, *24*, 287–310, 1995.
- McKane, R. B., E. B. Rastetter, G. R. Shaver, K. J. Nadelhoffer, A. E. Giblin, J. A. Laundre, and F. S. Chapin III, Climatic effects on tundra C storage inferred from experimental data and a model, *Ecology*, *78*, 1170–1187, 1997a.
- McKane, R. B., E. B. Rastetter, G. R. Shaver, K. J. Nadelhoffer, A. E. Giblin, J. A. Laundre, and F. S. Chapin III, Reconstruction and analysis of historical changes in carbon storage in Arctic tundra, *Ecology*, *78*, 1188–1198, 1997b.
- Mitchell, J. F. B., S. Manabe, V. Meleshko and T. Tokioka, Equilibrium climate change, in *Climate Change: The IPCC Scientific Assessment*, edited by J. T. Houghton et al., pp. 131–172, Cambridge Univ. Press, New York, 1990.
- Myneni, R. B., C. D. Keeling, C. J. Tucker, G. Asrar, and R. R. Nemani, Increased plant growth in the northern high latitudes from 1981 to 1991, *Nature*, *386*, 698–702, 1997.
- Nadelhoffer, K. J., L. Johnson, J. Laundre, A. E. Giblin, and G. R. Shaver, Fine root production and nutrient use in wet and moist arctic tundras as influenced by chronic fertilization, *Plant and Soil*, *242*, 107–113, 2002.
- Oechel, W. C., and W. D. Billings, Effects of global change on the carbon balance of arctic plants and ecosystems, in *Arctic Ecosystems in a Changing Climate: An Ecophysiological Perspective*, edited by F. S. Chapin III et al., pp. 139–168, Academic, San Diego, Calif., 1992.
- Oechel, W. C., and G. H. Riechers, Response of a tundra ecosystem to elevated atmospheric carbon dioxide, in *Response of Vegetation to Carbon Dioxide*, Rep. 037, U.S. Dept. of Energy, Carbon Dioxide Res. Div., Washington, D. C., 1987.
- Oechel, W. C., and B. R. Strain, Native species response to increased atmospheric CO₂ concentration, in *Direct Effects of Increasing Carbon Dioxide on Vegetation*, edited by B. R. Strain and J. D. Cure, pp. 117–154, DOE/ER-0238, Natl. Tech. Info. Serv., Springfield, Va., 1985.
- Oechel, W. C., G. H. Riechers, W. T. Lawrence, T. I. Prudhomme, G. L. Vourtilis, N. Grulke, and S. J. Hasting, “CO₂LT” an automated, null-balance system for studying the effects of elevated CO₂ and global change on unmanaged ecosystems, *Funct. Ecol.*, *6*, 86–100, 1992.
- Oechel, W. C., S. J. Hasting, G. L. Vourtilis, M. Jenkins, G. H. Riechers, and N. Grulke, Recent change of arctic tundra ecosystems from a net carbon dioxide sink to a source, *Nature*, *361*, 520–523, 1993.
- Oechel, W. C., G. L. Vourtilis, and S. J. Hastings, Cold season CO₂ emission from arctic soils, *Glob. Biogeochem. Cycles*, *11*, 163–172, 1997.
- Oechel, W. C., G. L. Vourtilis, S. J. Hastings, R. C. Zulueta, L. Hinzmann, and D. Kane, Acclimation of ecosystem CO₂ exchange in the Alaskan Arctic in response to decadal climate warming, *Nature*, *406*, 978–981, 2000.
- Potter, C. S., J. T. Randerson, C. B. Field, P. A. Matson, P. M. Vitousek, H. A. Mooney, and S. A. Klooster, Terrestrial ecosystem production: A process model based on global satellite and surface data, *Glob. Biogeochem. Cycles*, *7*, 811–841, 1993.
- Randerson, J. T., C. B. Field, I. Y. Fung, and P. P. Tans, Increases in early season ecosystem uptake explain recent changes in the seasonal cycle of atmospheric CO₂ at high northern latitude, *Geophys. Res. Lett.*, *26*, 2765–2768, 1999.
- Rastetter, E. B., Validating models of ecosystem response to global change, *Bioscience*, *46*, 190–198, 1996.
- Rastetter, E. B., and G. R. Shaver, A model of multiple-element limitation for acclimation vegetation, *Ecology*, *73*, 1157–1174, 1992.
- Rastetter, E. B., M. G. Ryan, G. R. Shaver, J. M. Melillo, K. J. Nadelhoffer, J. E. Hobbie, and J. D. Aber, A general biochemical model describing the responses of the C and N cycles in terrestrial ecosystems to changes in CO₂, climate, and N deposition, *Tree Physiol.*, *9*, 101–126, 1991.
- Rastetter, E. B., R. B. McKane, G. R. Shaver, and J. M. Melillo, Changes in C storage by terrestrial ecosystems: How C–N interactions restrict responses to CO₂ and temperature, *Water Air Soil Pollut.*, *64*, 327–344, 1992.
- Rastetter, E. B., R. B. McKane, G. R. Shaver, K. J. Nadelhoffer, A. E. Giblin, J. A. Laundre, and F. S. Chapin III, Analysis of CO₂, temperature and moisture effect on carbon storage in Alaskan arctic tundra using a general ecosystem model, in *Global Change and Arctic Terrestrial Ecosystems*, edited by W. C. Oechel et al., pp. 437–451, Springer-Verlag, New York, 1997.
- Reynolds, J. F., D. W. Hilbert, and P. R. Kemp, Scaling ecophysiology from the plant to the ecosystem: A conceptual framework, in *Scaling Physiological Processes: Leaf to Globe*, edited by J. R. Ehleringer and C. B. Field, pp. 127–140, Academic, San Diego, Calif., 1993.
- Shaver, G. R., and F. S. Chapin III, Production: Biomass relationships and element cycling in contrasting arctic vegetation types, *Ecol. Monogr.*, *61*, 1–31, 1991.
- Shaver, G. R., and S. Jonasson, Productivity of Arctic ecosystems, in *Terrestrial Global Productivity*, edited by H. Mooney et al., pp. 189–210, Academic, San Diego, Calif., 2001.
- Shaver, G. R., W. D. Billings, F. S. Chapin, A. E. Giblin, K. J. Nadelhoffer, W. C. Oechel, and E. B. Rastetter, Global change and the carbon balance of Arctic ecosystems, *Bioscience*, *42*, 433–441, 1992.
- Shaver, G. R., L. C. Johnson, D. H. Cades, G. Murray, J. A. Laundre, E. B. Rastetter, K. J. Nadelhoffer, and A. E. Giblin, Biomass and CO₂ flux in wet sedge tundras: Responses to nutrients, temperature and light, *Ecol. Monogr.*, *68*, 75–97, 1998.
- Silapaswan, C. S., D. L. Verbyla, and A. D. McGuire, Land cover change on the Seward Peninsula: The use of remote sensing to evaluate the potential influences of climate warming on historical vegetation dynamics, *Can. J. Remote Sens.*, *5*, 542–554, 2001.
- Sturm, M., C. Racine, and K. Tape, Climate change: Increasing shrub abundance in the Arctic, *Nature*, *411*, 546–547, 2001.
- Walker, M. D., D. A. Walker, and N. A. Auerbach, Plant communities of a tussock tundra landscape in the Brooks Range Foothills, Alaska, *J. Veg. Sci.*, *5*, 843–866, 1994.
- Williams, M., and E. B. Rastetter, Vegetation characteristics and primary productivity along an arctic transect: Implications for scaling-up, *J. Ecol.*, *87*, 885–898, 1999.
- Williams, M., E. B. Rastetter, D. N. Fernandes, M. L. Goulden, S. C. Wofsy, G. R. Shaver, J. M. Melillo, J. W. Munger, S. M. Fan, and K. J. Nadelhoffer, Modeling the soil–plant–atmosphere continuum in a *Quercus–Acer* stand at Harvard Forest: The regulation of stomatal conductance by light, nitrogen and soil/plant hydraulic properties, *Plant Cell Environ.*, *19*, 911–927, 1996.
- Williams, M., E. B. Rastetter, D. N. Fernandes, M. L. Goulden, G. R. Shaver, and L. C. Johnson, Predicting gross primary productivity in terrestrial ecosystems, *Ecol. Appl.*, *7*, 882–894, 1997.
- Williams, M., W. Eugster, E. B. Rastetter, J. McFadden, and F. S. Chapin III, The controls on net ecosystem productivity along an Arctic transect: A model comparison with flux measurements, *Global Change Biol.*, *6*, 116–123, 2000.
- Williams, M., E. B. Rastetter, G. R. Shaver, J. H. Hobbie, E. Carpino, and B. L. Kwiatkowski, Primary production in an arctic watershed: An uncertainty analysis, *Ecol. Appl.*, *11*, 1800–1816, 2001.
- Zhou, L., C. J. Tucker, R. K. Kaufmann, D. Slayback, N. V. Shabanov, and R. B. Myneni, Variations in northern vegetation activity inferred from satellite data of vegetation index during 1981 to 1999, *J. Geophys. Res.*, *106*, 20,069–20,083, 2001.

S. Daeschner, A. Hope, and D. Stow, Department of Geography, San Diego State University, San Diego, CA 92182, USA.

J. E. Hobbie, B. L. Kwiatkowski, S. Le Dizès, and E. B. Rastetter, The Ecosystems Center, Marine Biological Laboratory, Woods Hole, MA 02543, USA.